Non-oxidative Methane Activation Over Molybdenum and Tungsten Nitrides

Presented by
Mohsen Shahryari
Department of Chemical Engineering

McGill University Montreal, Canada
August 2021

A thesis submitted to McGill University in partial fulfillment of the requirements of the degree of Master of Science

Supervisor:

Prof. Dr. Sc. Jan Kopyscinski (McGill University, Chemical Engineering).

Acknowledgments

Wayne Gretzky once said, “I skate to where the puck is going, not where it has been.” This quote perfectly summarizes the mental and emotional transformation I have gone through in this fruitful journey towards gaining my master’s degree. It made me look forward. This transformation was largely due to the following people who generously gave me their time and efforts to assist me.

I am deeply grateful to my supervisor Dr. Jan Kopyscinski for accepting me as a student and giving me the opportunity to work in his group. I would not have succeeded if it was not for his support and constant encouragement to do better.

A big thanks to all the members of the catalytic processing and plasma engineering group (CPPE), who were always available as friends. In addition, a special thanks to Kanchan Dutta, whose patience and support as a mentor helped me learn and understand the tools required for my research. He was kind enough to support me even after his graduation. I consider him a good friend. Moreover, a big token of gratitude to Mohammad Ghavipour for his kind support, valuable feedback, and fruitful discussions regarding my experiments. Andrew Carkner was readily available and helped with my questions, for which I am grateful. Likewise, a big thanks to Elmira Pajootan for going above and beyond in answering my questions, performing some characterization tests, and also providing valuable feedback.

I would like to also extend my gratitude to the technical and administrative staff of McGill’s Chemical Engineering Department for their help and advice. Many thanks to Frank Caporuscio, Lou Cousmich, Andrew Golsztajn, Gerald Lepkyj, and Ranjan Roy for the technical assistance, and Lisa Volpato & Louise Miller-Aspin for their help in the administrative duties. I would like to thank McGill University,

Eugenie Ulmer-Lamothe (EUL) scholarship and my supervisor for their financial support during my master's degree.

I owe a huge debt of gratitude to my parents and siblings for their constant support, encouragement, and guidance throughout my life. Thank you to my entire family for always encouraging me to pursue my master's degree. And most of all, all success is due to The Creator.

Abstract

The abundance of natural gas (methane) has gained enormous attention towards its use as a feedstock replacement in petrochemical industries. Canada is one world's top chemical and plastic manufacturing industries. Ethylene and aromatics are used largely (52% and 30% respectively) as feedstocks in petrochemical industries. Due to volatile oil price and its depletion, it makes it essential for refiners to look for a reliable feed replacement for optimum revenue, making methane gas a good candidate.

Direct non-oxidative conversion of methane to olefins and aromatics can be a potential alternative to the conventional intermediate synthesis-gas production route. This process does not produce greenhouse gas and could also be used for clean hydrogen gas production. However, activation of the C–H bonds in CH_4 is extremely challenging and thermodynamically limited, requiring high temperatures (700–1000°C) and an efficient catalyst. Also, selectivity and coking of the catalyst are considered a major challenge. Many rare and expensive metal oxides have been studied as a catalyst with molybdenum oxides on zeolites studied the most. This research focuses on molybdenum (Mo), tungsten (W), and gallium (Ga) catalysts.

In this master's thesis, the metal catalysts chosen are gallium (Ga), molybdenum (Mo), and tungsten (W). Each of these metals has shown to be active towards methane activation. Metal nitrides are an

alternative to noble-metal catalysts; our group has recently reported catalytic activity of gallium nitride towards methane activation. In this study, the catalytic performance of molybdenum, tungsten, and mixed-metal molybdenum/tungsten nitrides was investigated. The effect of atomic ratios of molybdenum and tungsten on the methane conversion, product selectivity, and coke formation was evaluated. The study on gallium nitride catalyst and its regeneration capability was studied as collaborative work.

The metal and mixed-metal nitride catalysts were synthesized via impregnation of the corresponding precursors onto silica support (SBA-15) with a total target metal loading of 4 wt% and varying atomic ratios between Mo and W. Impregnated catalysts were dried and subsequently calcined at 750°C to form metal oxides. Prior to the methane activation experiments, the metal oxides were either reduced in H_2 at the 700°C for 1 h or nitridated under NH_3 gas at 700°C for 3 h to form the corresponding metal nitrides. Reduction, nitridation, and activity experiments were carried out in the same fixed bed reactor setup at the same temperature (700°C) and a gas hourly spaced velocity (GHSV) of 1160 h^{-1} at 1 bar_{abs}. The product gas mixture was analyzed via a calibrated mass spectrometer, while the amount of coke was determined via temperature-programmed oxidation in a thermogravimetric analyzer (TGA). The catalysts were characterized using N_2 adsorption/desorption, chemisorption, diffuse reflectance infrared Fourier transform spectroscopy (DRIFTS), X-ray diffraction (XRD), scanning electron microscopy and energy-dispersive X-ray spectroscopy (SEM-EDS), and X-ray photoelectron spectroscopy (XPS) to understand the structure-activity relationship.

The methane conversion to hydrocarbons along with the coke formation and product selectivity of the catalysts were evaluated. Mo, W, and MoW catalysts have higher activity than the corresponding nitrides with Mo and MoN achieving a CH_4 conversion to hydrocarbon values of 0.85 % and 0.55%, respectively. W and WN catalysts are slightly less active with CH_4 conversions of 0.55% and 0.14%, respectively. Despite the lower CH_4 conversion, the metal nitrides have a much lower coke formation and a much higher selectivity towards ethylene as aromatic species are more prone for coke formation. The lowest coke deposition was 8 $mg_{Coke}\ g_{Cat}^{-1}$ on WN/SBA-15 for the nitride compared to 110 $mg_{Coke}\ g_{Cat}^{-1}$ for the metal catalysts. The C_2H_4 selectivity is greatly increased with the relative amount of tungsten. Mo and MoN achieve C_2H_4 selectivity of 10% and almost zero, respectively, while W and WN achieve 25% and 42% C_2H_4 selectivity. The highest C_2H_4 selectivity of 65% was reached with the mixed-metal nitride catalyst containing Mo:W ratio of 5:1. Using TGA, it was shown that the gallium nitride (GaN) catalyst could be successfully regenerated with air while maintaining a stable ethylene yield. The DRIFTS experiments confirmed the DFT work that ethylene is formed first followed by benzene formation over gallium in non-oxidative CH_4 conversion.

Résumé

L'abondance de gaz naturel (méthane) reçoit énormément d'attention comme substitut de matériel-brut dans l'industrie pétrochimique. Canada est un des producteurs les plus importants de produits chimiques et de plastique. Éthylène et aromatiques sont les principaux matériaux-brut (52% et 30%) dans l'industrie petrochimique. À cause de la volatilité du prix et l'épuisement de stock de pétrole, c'est primordial que les raffineries cherchent une source fiable pour optimiser leur revenu : ce qui rend le méthane un bon candidat.

La conversion directe non-oxidative de méthane en olefins et aromatiques est une alternative potentielle au processus traditionnel par gaz de synthèse. Ce process ne produit pas de gaz à effet de serre et permet la production propre d'hydrogène. Pourtant l'activation des liens C-H du CH_4 est un défi et est limité thermodynamiquement, ce que requiert de températures élevées (700–1000°C) et un catalyseur efficace. La sélectivité et cokéfication du catalyseur sont aussi de défis importants. Maintes oxides de métaux rares et chers ont été étudiés, surtout les oxides de molybdenum sur zéolites. Ce recherche vise des catalyseurs de molybdenum, tungsten et gallium.

Dans cette thèse de Maîtrise, les catalyseurs choisis sont gallium (Ga), molybdenum (Mo) et tungsten (W). Chacun s'est démontré actif envers l'activation de méthane. Les nitrides de métal sont une

alternative aux catalyseurs de métal-noble : récemment, notre groupe a publié l'activité catalytique de nitride de gallium envers l'activation de méthane. La performance catalytique de nitrides de molybdenum, tungsten et mélanges molybdenum-tungsten ont été investigués. L'effet du ratio atomique de molybdenum et tungsten sur la conversion, sélectivité et formation de coke a été évalué. Le catalyseur nitride de gallium, ainsi que sa capacité régénératrice, ont été étudié de manière collaborative.

Les nitrides de métaux et métaux mixtes ont été synthétisé via imprégnation des précurseurs sur un support de silice (SBA-15) dont le taux massique cible a été 4% avec une plage de ratios Mo/W. Les catalyseurs imprégnés ont été séchés et ensuite calcinés à 750°C pour former des oxides de métal. Avant les expériments d'activation de méthane, les oxides de métal ont été réduit par H_2 à 700°C pour 1 h or nitridé par NH_3 à 700°C pour 3 h pour former le nitride de métal correspondant. La réduction, nitridation et tests d'activité ont tous été fait dans le même réacteur à lit fixe et à la même température de 700°C avec charge de catalyseur de 200 mg et un GHSV (*gas hour spaced velocity* en anglais) de 1160 h^{-1} à 1 bar_{abs}. Le mélange de gaz produit a été analysé via spectromètre massique calibré et la quantité de coke par oxidation par température programmé dans un TGA (*thermogravimetric analyzer*). Les catalyseurs ont été caractérisés par adsorption/desorption N_2, chemisorption, DRIFTS (*diffuse reflectance infrared Fourier transform spectroscopy*), XRD (*X-ray diffraction*), SEM-EDS (*scanning electron microscopy and energy-dispersive X-ray spectroscopy*) et XPS (*X-ray photoelectron spectroscopy*) pour comprendre la relation structure-activité.

La conversion de méthane en hydrocarbure avec formation de coke et sélectivité de produits des catalyseurs ont été évalués. Mo, W et MoW ont une activité plus élevés que les nitrides correspondants : Mo et MoN ont atteint une conversion de CH_4 en hydrocarbure de 0.85 % et 0.55%. W et WN sont légèrement moins actifs, avec conversions de CH_4 de 0.55% et 0.14%. Malgré la moindre conversion de CH_4, les nitrides de métaux forment beaucoup moins de coke et ont une sélectivité plus élevé envers éthylène tandis que les aromatiques sont plus propices pour la formation de coke. Le moindre déposition de coke a été 8 $mg_{Coke}\ g_{Cat}^{-1}$ sur WN/SBA-15 pour les nitrides comparé avec 110 $mg_{Coke}\ g_{Cat}^{-1}$ pour les métaux. La sélectivité de C_2H_4 augmente de manière importante avec une augmentation du taux de tungsten. Mo et MoN ont atteint une sélectivité envers C_2H_4 de 10% et presque zéro, tandis que W et WN ont eu des sélectivités de C_2H_4 de 25 and 42%. La sélectivité la plus haute, 65%, a été atteint avec un catalyseur nitridé de métaux mixtes avec un ratio Mo:W de 5:1. Les résultats TGA ont démontrés que le catalyseur nitride de gallium (GaN) peut être regénéré avec de l'air en maintenant un rendement stable d'éthylène. Les tests DRIFTS ont confirmé les résultats des calculs DFT qu'éthylène est formé d'abord suivi de benzène sur gallium avec conversion non-oxidative de CH_4.

Table of Content

Chapter 1

1 Introduction

1.1 Motivation

Natural and shale gases are available abundantly with the main constituent being methane [1]. The world natural gas reserves found are estimated at 7, 257 trillion cubic ft as of 2020 [2]. Canada ranks among the top six in the production and exporting of natural gas [3]. Also in Quebec, natural gas reserves estimated to be between 250 to 1150 billion cubic meters are found in the southern part of the St. Lawrence valley which could fulfill Quebec's natural gas demand for at least 40 more years [4]. The oil and gas contribute to the raw material to produce chemicals such as olefins like ethylene, propylene, and butadiene, and the aromatics like benzene, toluene, and xylenes. The volatile oil price from various geopolitical reasons and that its depletion affects the price of petrochemicals and hence revenue. Thus, deriving manufacturers towards the replacement of feedstocks with natural gas for a reliable feedstock for optimum revenue and growth rate for higher profit margins. This also helps with a more stable price for end-users of the petrochemicals. Thus, moving towards the conversion of methane (CH_4), which is the main component of natural gas to useful chemicals such as olefins and aromatics would be a topic of interest and has attracted researchers.

Aromatics, olefins, and hydrogen are useful products that can be derived from methane gas through the process of dehydrogenation [5]. One of the major interests of catalytic conversion of methane is to convert methane gas into useful products onsite into higher hydrocarbons to reduce transportation costs. This is because most processing sites are located in remote areas and transportation costs could be significant [1]. Canada's petrochemical industry is dominated by ethylene production, which is an olefin and products derived from it [6]. A total of $9.7 billion was reported for Canada's plastic and resin manufacturing industry, where ethylene is a crucial building block [7]. In Canada, 58.6% of its revenue comes from ethylene production which is produced in Alberta, Ontario, and Quebec provinces [8]. Ethylene is required to produce precursors such as polyethylene (50%), ethylene oxide (10%), and other chemicals such as ethylene glycol. Vinyl acetate, polyvinyl chloride, polyester with many alcohols and solvents are also amongst the products that require ethylene for their production. The Current production of ethylene is through stream cracking of hydrocarbons that included naphtha, gas oil, and condensates. This process thus produces other hydrocarbons such as propylene, C_4 olefins, aromatics, and pyrolysis gasoline.

Catalytic processes for converting methane conversion include (1) indirect oxidative, (2) direct non-oxidative, and (3) indirect non-oxidative dehydrogenation [5–7]. The current practices used are the Fischer tropsch and methanol synthesis which are examples of indirect oxidative routes done through partial oxidation or reforming to syngas (CO, H_2) followed by coupling reactions. The downside with these processes is that they require high capital cost, are low in efficiency, and produce CO_2 in the outlet stream. Fig. 1-1 shows the products derived from the direct and indirect conversion of methane.

The oxidative route is an exothermic reaction that uses oxidants such as air and steam [1]. CO and CO_2 are the primary products in oxidative dehydroaromatization (DHA) with low selectivity for aromatics [9], [10].

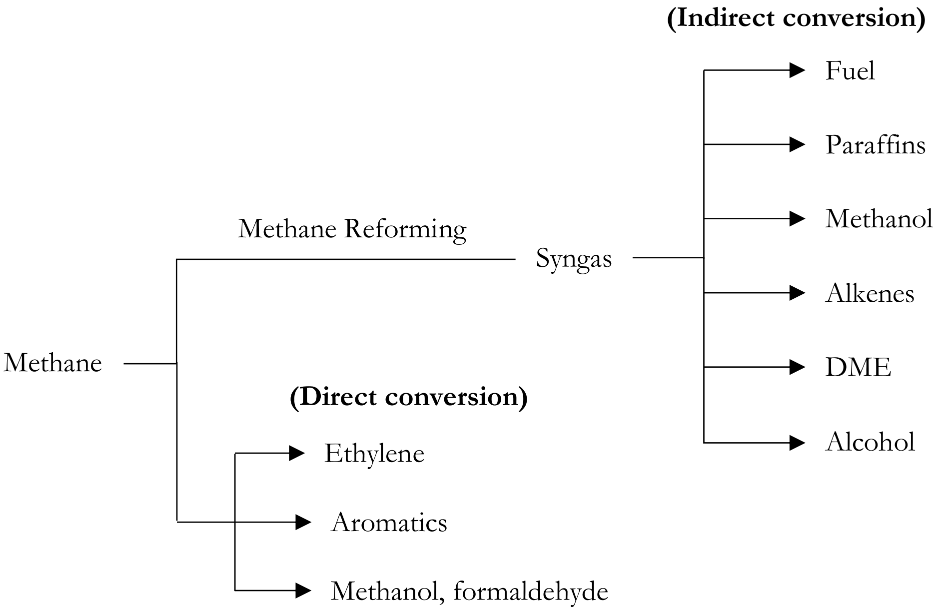

Fig. 1-1: Direct and indirect route for methane conversion adapted from [10].

Although direct oxidative methane conversion is not thermodynamically limited ($\Delta G < 0$ kJ mol^{-1}), the process has a low yield since the products are more reactive than the reactant and can oxidize to form CO_2 [11,12]. Direct non-oxidative conversion has thermodynamic constraints, i.e., $\Delta G > 0$ kJ mol^{-1} with low CH_4 conversion, and kinetic limitations of low selectivity and high coke formation. This process of converting methane to higher hydrocarbons and hydrogen gas is an endothermic process and demands high energy input (700−1000°C), an efficient catalyst and reactor engineering are required [1] [13,14].

The metal and metal oxide catalysts have been widely studied during the past two decades for methane activation [10,12,14–20]. To mention a few, bifunctional metals modified zeolites were studied by Profs. Kapteijn [20], Spivey [18], Hensen [16], Lobo [17], Dumesic [21], Varma [22], Khatib [23]. The activation of methane involves C–H bond cleavage over the metal to form CH_x surface species and subsequent C–C coupling. This is followed by cyclization, which could happen at high temperatures in the gas phase (>950 °C) or is believed to happen on the Brønsted acid sites of the zeolite support, which also causes to form coke on the surface of the catalyst [10,18]. In general, most catalysts are metal oxides, and it is a common belief that acidity/basicity (Lewis acid/base pairs) plays a wide role in C–H bond activation.

Metal nitrides catalysts have been investigated to a lesser extent, but have shown catalytic activity similar to precious metal catalysts [24]. For instance, nitride catalysts are used in ammonia synthesis, selective hydrogenation, and hydrotreating [25]. In Dr. Kopyscinski's group, a former PhD student (Kanchan Dutta) investigated unsupported and supported gallium oxide and gallium nitride catalysts for the non-oxidative methane activation and showed promising results. As gallium is extensively used in the semiconductor industry it might not be an economically viable material as a catalyst. Therefore, it is of great interest to investigate other metal nitrides such as molybdenum and tungsten for the non-oxidative methane activation.

1.2 Objectives

The objective of this study was to investigate molybdenum, tungsten, and their mixed-metal supported on SBA-15 for the non-oxidative methane conversion. In detail, this work aims to shed light on the structure-activity relationship and possible synergistic effect of the mixed metal nitrides on methane conversion and product selectivity. In order to achieve the objective, the following sub-objectives and tasks are defined:

1. Investigate the relationship between catalyst synthesis and its structure for single and mixed metals, metal oxides, and metal nitrides.
2. Study the effect of nitridation on catalyst activity and selectivity.
3. Study the effect of Mo:W ratio catalyst activity and selectivity.

1.3 Organization of the thesis

The thesis is divided into three main sections: theoretical background, experimental procedure, and presentation and discussion of the results. The organization of the thesis is as follows:

Chapter 2 provides a short theoretical background on direct non-oxidative methane activation, summarizes catalysts used, and briefly discusses the reaction mechanism.

Chapter 3 outlines the methodology for the catalyst preparation, characterization techniques, and the experimental setup for the activity measurements.

Chapter 4 presents and discusses the collaborative work done on gallium nitride catalyst used for the non-oxidative methane activation.

Chapter 5 presents and discusses the results for molybdenum, tungsten, and their mixed-metal catalysts for the non-oxidative methane activation.

Chapter 6 draws the conclusion and provides recommendations for further improvements and developments for future research.

1.4 Contribution

The author of the thesis was responsible for the literature review, design experiments, catalyst synthesis, and analysis of the results. Elmira Pajootan performed characterization tests (SEM, XRD, XPS) and assisted in the analysis of the work. Dr. Kopyscinski reviewed the thesis and provided feedback on the analysis, structuring, and formatting of the thesis.

Chapter 2

2 Theoretical background

Methane gas's main sources are natural gas, shale gas, and biogas and with its abundancy has a great potential of replacing feedstocks for the synthesis of chemicals and building blocks. The non-oxidative methane conversion using heterogeneous catalysts has gained attention and could be a potential route for industrial application. Many reviews have been published in the last two decades [1,12,13,18,26–29] with the main emphasis on catalysts design and reactor concepts for the production of aromatics. Yet, there is not much research on the direct coupling of methane to olefins such as ethylene. This chapter will summarize the chemistry, thermodynamics, and catalyst concepts.

2.1 Chemistry and thermodynamics

The direct non-oxidative methane coupling to ethylene and benzene is presented by eqs. 2−1 and 2−2:

$$CH_4 \leftrightarrow \frac{1}{2} C_2H_4 + 2 H_2 \qquad \Delta G_R^o = 85\ kJ\ mol^{-1} \qquad \Delta H_R^o = 101\ kJ\ mol^{-1} \qquad 2{-}1$$

$$CH_4 \leftrightarrow {}^{1}/_{6}\, C_6H_6 + {}^{3}/_{2}\, H_2 \qquad \Delta G_R^o = 72\ kJ\ mol^{-1} \qquad \Delta H_R^o = 88\ kJ\ mol^{-1} \qquad 2{-}2$$

These reactions are endothermic and thermodynamically unfavorable indicated by the positive heat of reaction and Gibbs free energy, respectively. Methane can also be pyrolyzed to C and H_2 via eq. 2−3:

$$CH_4 \leftrightarrow C + 2 H_2 \qquad \Delta G_R^o = 51\ kJ\ mol^{-1} \qquad \Delta H_R^o = 75\ kJ\ mol^{-1} \qquad 2{-}3$$

Thermodynamically, when coke formation is excluded, the maximum achievable CH_4 conversion and C_2H_4 yield are 4.1% and 3.5% at 700 °C, 9.1% and 8.1% at 800 °C, and 17.0% and 15.5% at 900 °C, (Fig. 2-1A). Once benzene is included in the equation, the selectivity shifts towards benzene (Fig. 2-1B), with ethylene yield lowering to 0.18%. The reason is due to resonance and π−electron cloud delocalization that makes benzene a more stable product [30]. The calculations were done with the software tool HSC Chemistry v9.

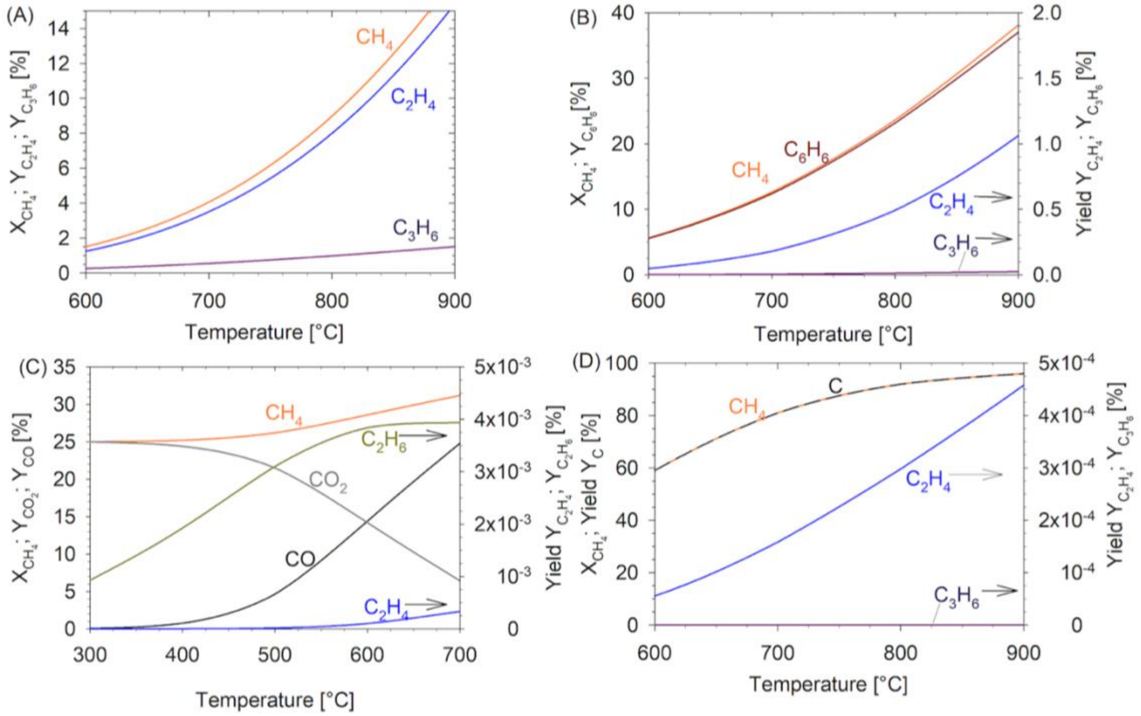

Fig. 2-1: (A) CH_4 equilibrium conversion and C_2H_4, C_3H_6 yields, (B) CH_4 equilibrium conversion and C_6H_6, C_2H_4, and C_3H_6 yields, (C) CH_4 equilibrium conversion and CO, CO_2, C_2H_6, and C_2H_4 yields for the oxidative coupling of methane (OCM with $CH_4/O_2 = 2$) as a function of temperature at 1 bar, and (D) CH_4 equilibrium conversion (non-oxidative) and C_2H_4, C_3H_6 yields with carbon as one of the products [31].

For the oxidative methane conversion, a CH_4 to O_2 ratio of 2 [32] and CO, CO_2, H_2O, C_2H_6, and C_2H_4 as possible products were assumed for the thermodynamic equilibrium calculations (Fig. 2-1C). As mentioned earlier, the oxidative although is not thermodynamically limited and has higher conversion. However, the main products are undesired carbon oxides (CO and CO_2) with negligible desired products (C_2H_4 and C_2H_6, Yield < 0.01%), which results in lower carbon efficiency.

The non-oxidative conversion pathway does not produce any CO_2 and can be considered more environmentally friendly. However, as discussed above, there are huge drawbacks due to thermodynamic and kinetic limitations. Regarding the latter, coke formation especially at high temperature (>750 C) is significant and leads to catalyst deactivation as well as negatively affects the selectivity [33]. Thus, when the carbon deposition was added to the equilibrium calculations, the reaction favored mainly coke with negligible desired products (Fig. 2-1D). The formation of coke could be due to the pyrolysis reaction of methane or due to the formation of adsorbed intermediated C_xH_y species with the release of H_2.

2.2 Catalyst

The reaction mechanism, surface intermediates, and rate-limiting steps are complex and not well understood over metal nitrides and still controversial over metal and metal-oxide catalysts. CH_4 has a very stable C–H bond, which is difficult to activate under non-oxidative environment [14]. For example, methane aromatization on metal-modified zeolites is widely studied with the research work summarized in articles from Ma *et al.* [10], Spivey and Hutchings [18], and Karakaya and Kee [13]. Metals such as Mo, Zn, W, Re, Cu, Mn, Ni, and Cr have been investigated, with molybdenum-containing zeolites exhibiting the highest activity in terms of methane conversion (3−16%) with benzene (50−75%) as the main product [14]. It is assumed that Mo catalysts are bifunctional with the initial steps in the reaction involving the reduction of molybdenum oxide to Mo-carbide (Mo_2C) by CH_4 where C–H are broken to form the reactive $–CH_x$. This is followed by dimerization to form C_2H_y which further oligomerizes and cyclizes to form C_6H_6 and release H_2 (Fig. 2-2). It is believed that the Brønsted acid sites are where the oligomerization and cyclization take place. Although, the detailed

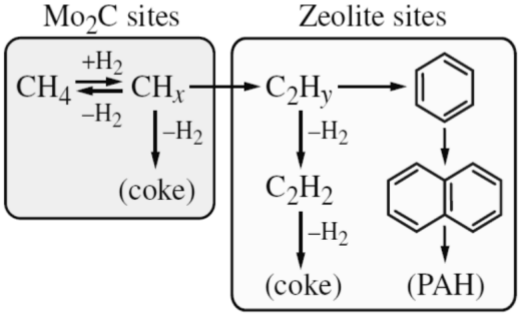

Fig. 2-2: Reaction mechanism for non-oxidative CH4 aromatization, adapted from [13].

mechanism of dimerization and oligomerization are yet to be understood [10,13]. Coke formation is inevitable under the non-oxidative environment with CH_4 and high temperature which is believed to form from $–CH_x$ and C_2H_y complexes. Toluene is formed when a benzene ring is combined with a CH_2 or CH_3 active species. Naphthalene can be formed as a result of two phenyl groups joining [21]. Further combination of phenyl species can lead to the deactivation of the catalysts by forming polynuclear aromatic compounds referred to as coke.

It is shown that the addition of metals as promoters can have positive effects on methane activation. Improvements in methane conversion, product selectivity, and catalyst stability are shown by transition elements in period 4 (Fe, Co, Ni, and Cr) and metals in group 13 (Ga and Al) of the periodic table [10].

There is less published research available on the non-oxidative conversions of methane to light hydrocarbons and olefins than for methane aromatization [34]. For instance, in a recent study done by Dumesic's group, they developed a PtSn/zeolite and with coke being excluded achieved C_2H_4 selectivity of (70–90%) and conversion of < 0.5% (product based) at 700 °C; yet coke production remained as the main concern [21]. Under similar conditions, Xiao and Varma [22] achieved a C_2H_6 selectivity of 90% (excluding coke) and conversion of 1–5% on bimetallic PtBi/zeolite. However, they reported a 10% selectivity towards C_2H_4 and 40–50% coke selectivity on 1% Pt−0.2% Bi catalyst at 650 °C with 0.1 atm CH_4 partial pressure. Moreover, they suggested that coke formation was during the early activation period. Bajec *et al.* [34] investigated the methane activation and coupling to ethane and ethylene on Fe/HZSM-5, Mo/HZSM-5, and FeMo/HZSM-5 and were able to achieve 50% C_2H_4 selectivity, 1–6% CH_4 conversion, and 11–35 wt% coke at 700 °C, WHSV of 2 h^{-1}, p_{tot} of 1.5 bar. The effect of support acidity was also observed in Sheng *et al.* [17] where a less acidic boron-based zeolite produced less coke with 90% selectivity (gas phase) towards C_2H_4 and less than 1% conversion at 700 °C. Single iron sites embedded in silica were synthesized by Guo *et al.* [15] that produced minimum coke deposition with 48% C_2H_4 selectivity and a conversion of 48% at a temperature of 1090 °C. Lee *et al.* [35] studied methane activation at 650 °C with 0–7 wt% Ga loading and a GHSV of 6000 ml g_{cat}^{-1} h^{-1} with ethane as co-feed. They were able to achieve a conversion of 0.3–6% (methane and ethane), 25–30% ethylene and 15–30% benzene selectivity, and 45–60% coke. Dipu affected methane activation with Ni catalyst on silica by adding a second phosphorous element [36]. It was found the bimetallic catalyst (NiP/SiO_2) to active towards methane activation at 900 °C. The resulting selectivity for C_2H_4 was around 60% and conversion of 3%. The range of products were C_2H_4 (ethylene), C_2H_6 (ethane), C_2H_2 (acetylene), C_3H_6 (propylene), C_6H_6 (benzene), C_7H_8 (toluene) and $C_{10}H_8$ (naphthalene). In Dr. Kopyscinski's group, GaN catalyst was developed that showed high selectivity towards C_2H_4 [37].

2.3 Reaction mechanism

A step-based kinetic model for the steady-state reaction for converting methane to aromatics was developed by Wong *et al.* [38]. It is assumed that it starts with the formation of C_2H_4 on the Mo sites and then oligomerization to benzene on the acid sites.

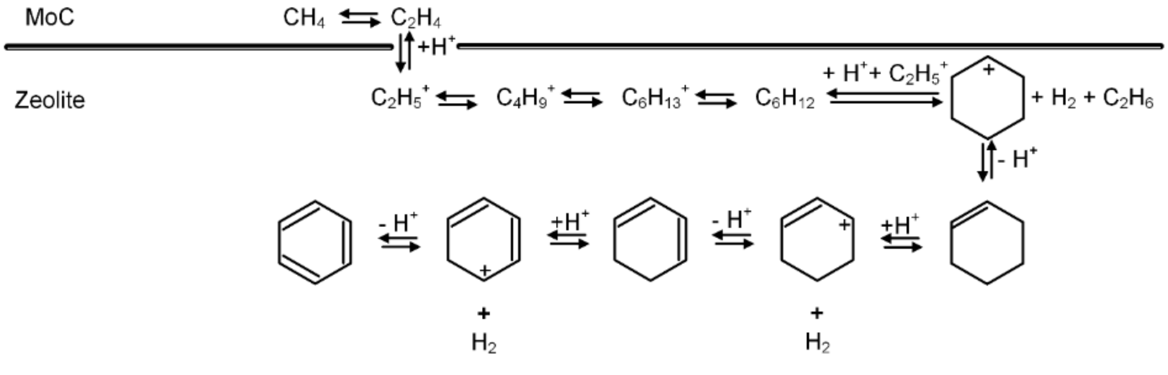

Fig. 2-3: Elementary steps for CH_4 activation over the Mo/HZSM5 catalyst, adapted from [38].

The acid-catalyzed elementary steps are grouped into chemisorption, desorption, oligomerization, β−scission, hydride transfer, protolytic dehydrogenation and hydrogenation, protolysis, alkylation and dealkylation of toluene and naphthalene [39].

The study by Luzgin *et al.* on Ga modified zeolites showed that dissociative adsorption of methane on Ga_2O_3 species could happen via "alkyl" pathway ($Ga-CH_3$) forming gallium-methyl or the carbenium mechanism forming the gallium-methoxy groups ($Ga{\cdot}O-CH_3$). The methoxy mechanism happens to a lesser extent, however, the addition of molecular oxygen could increase it through partial oxidation [40].

The methane adsorption model was first reported by Li *et al.* [41] using DFT showing that CH_4 adsorbs through the alkyl adsorption path on the m-plane consisting of GaN with equal ratios. The CH_4 is dissociatively adsorbed with its carbon atom attracted to the Ga^{3+} (blue atoms in Fig. 2-4A) and an H to the N^{3-} anion (orange atoms in Fig. 2-4A) with the remaining three other H atoms on the opposite side [42] Based on experiments and DFT modeling, it is suggested that the rate-limited step is the second C−H bond cleavage to form CH_2*, which then reacts with an adjacent CH_2* species to C_2H_4 (Fig. 2-4). CH_2* can further be dehydrogenated to form undesired coke.

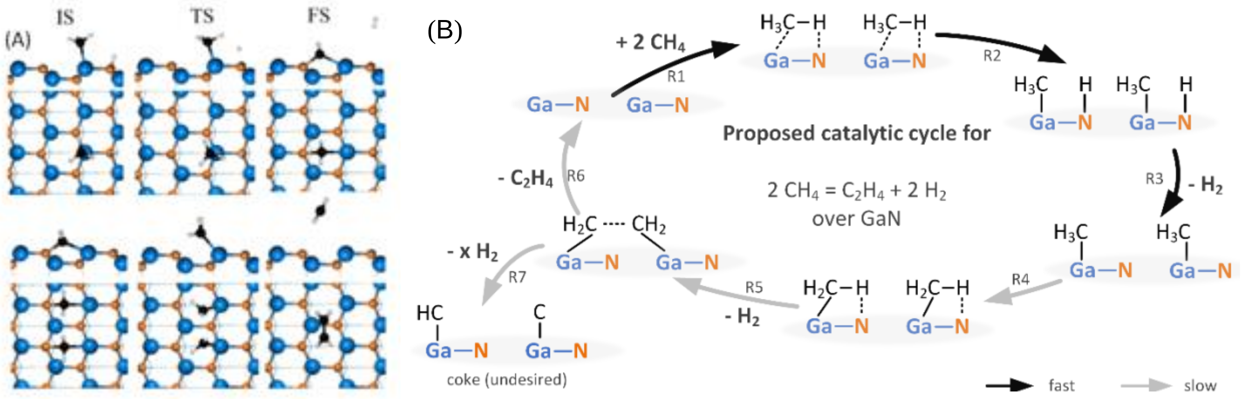

Fig. 2-4 Proposed reaction mechanism from methane to ethylene over GaN catalyst, adapted from [42].

Chapter 3

3 Methodology

3.1 Catalyst preparation

Within this thesis, a set of Gallium, Molybdenum, and Tungsten-based catalysts (i.e., metals, metal oxides, metal nitrides, supported and unsupported) were developed, characterized, and tested.

3.1.1 Gallium catalysts

Unsupported gallium-catalyst was prepared by the Evaporation Induced Self Assembly (EISA) as developed by our research group and described in Chaudhari *et al.* [42]. In detail, 1 g of a triblock copolymer (Pluronic P-123, Sigma Aldrich) was dissolved in 16 ml of pure anhydrous ethanol (Greenfield Global Inc.) until a homogeneous solution was obtained. This was followed by the addition of 1.7 ml of nitric acid (67−70 wt%, Fisher Scientific) and stirring for complete mixing with the acid. To the copolymer solution, another solution containing 4.5 g of dry gallium(III)nitrate hydrate powder in 5 ml DI-water and 5 ml of ethanol was added. The solution was then stirred for 5 h at 600 rpm at room temperature. The homogeneous, colorless mixture was kept inside a drying oven at 60 °C for 48 h. After that, the dried copolymer-gallium mixture was calcined at 650 °C for 6 h at a heating rate of 1 °C min^{-1} in which the copolymer was burned, and the gallium-precursor was converted to Ga_2O_3.

For the supported catalyst, ordered mesoporous silica (SBA−15) was synthesized as described in [37,43]. Around 4 g of a triblock copolymer (Pluronic P-123, Sigma Aldrich) was dissolved by stirring (600 rpm for 5 h) in 95 ml of deionized water until a homogeneous solution was obtained. To this solution, 4 ml of hydrochloric acid (HCl, 37 wt%, Fisher Scientific) was added and stirred for about 15 min at a temperature of 38 °C. Then 9.5 ml of tetraethoxysilane (TEOS, 99.9%, Alfa Aesar) was added. The resulting mixture was stirred at 600 rpm for an additional 24 h at 38 °C for completing TEOS hydrolysis and precipitation of silica. The mixture was then placed inside a closed polypropylene digestion DigiTUBEs (SCP science) and kept inside an oven at 100 °C for 48 h for hydrothermal treatment. After cooling down, the white powder was separated by filtration and washed with deionized water several times, followed by overnight drying at 60 °C. Finally, SBA−15 was obtained by calcining the dried solid at 550 °C for 5 h at a heating rate of 1 °C min^{-1}.

Gallium was added via incipient wetness impregnation (IWI) to SBA−15 with a target loading of 16 wt%. Typically, 1 g of SBA−15 was impregnated with 1 g of gallium (III) nitrate hydrate in a 4.5 ml aqueous solution. The almost wet solid was left for 24 h at room temperature followed by drying overnight at 70 °C. The dried solid was then calcined at 550 °C for 5 h at a heating rate of 1 °C min^{-1} to produce gallium oxide inside SBA−15 with a target Ga loading of 16 wt%.

Unsupported and supported nitride catalysts (denoted GaN and GaN/SBA-15), as well as nitridated support (N-SBA15), were prepared via nitridation of the parent sample with anhydrous ammonia (NH_3, 99.99%, Linde). The nitridation was carried out prior to the activity test in the same packed bed reactor. By doing so, exposure to air was avoided, and no surface oxygen was present. The nitridation was done at 700 °C for the Ga_2O_3/SBA15 and 750 °C for the Ga_2O_3 sample using 15 ml_N min^{-1} NH_3 and 1 ml_N min^{-1} Ar for 11 h.

3.1.2 Molybdenum and tungsten catalysts

Molybdenum, tungsten, and their corresponding mixed metal catalysts were only synthesized on silica support (SBA-15). Two batches of SBA-15 were prepared, batch 1 (B1) and batch 2 (B2). The synthesis procedure for the SBA-15's (B1 and B2) was slightly adjusted to the method described above in order to get a more precise synthesis. The changes include slightly higher acid composition (Table 3-1), the higher temperature during mixing (57 °C for B1 and B2, compared to 38 °C in the previous batch), and incorporation of a syringe pump for gradual addition of reagents. For the preparation of B1, slightly more acid (HCl) was used, and the first mixing stage time was less (8 h compared to overnight, Fig. 3-1) compared to B2, these changes resulted in a slightly higher BET surface area (~100 $m^2\ g^{-1}$), Table 5-1.

Table 3-1: Gel composition for SBA-15 synthesis and mixing temperature.

Method	**Gel composition [mol]**	**TEOS [mol]**	**P-123 [mol]**	**HCl [mol]**	**H_2O [mol]**	**Temperature [°C]**
Previous method	Actual [mol]	0.20	0.003	0.22	24	38
	Actual [g]	41.67	18.560	21.68	432	
Current method (B2)	Actual [mol]	0.20	0.003	0.30	24	57
	Actual [g]	41.70	17.400	29.60	432	

The molybdenum, tungsten, and their mixed metal catalysts were prepared the same way as the gallium catalysts explained above. Ammonium molybdate (VI) tetrahydrate (99+%, ACROS Organics, fisher scientific) and Ammonium Metatungstate Hydrate (99.99% trace metals basis, Sigma Aldrich) were used as precursors for molybdenum and tungsten catalysts respectively. Prior to impregnation, the metal solutions were prepared with DI water in a vial and left overnight to ensure complete dissolution of the metal precursors. Typically, 4.5 ml of DI water was used to impregnated 1 g of the SBA-15 support with the precursor of the desired metal or mixed metals. The impregnated support was bench dried at room temperature for 4 h and then drying in a muffle furnace at 90 °C for 5 h (heating rate of

2 °C min^{-1}) followed by subsequent calcination at 750 °C at a heating rate of 2 °C min^{-1} to produce the metal or mixed metal oxide catalysts on SBA-15 support. Since pre-treatments (reduction under H_2 and nitridation under NH_3) and activity tests (with CH_4) were performed at 700 °C, the final calcination was done at 750 °C to eliminate any effect that could arise from temperature increases such as pore collapse on BET as illustrated in section 5.2.1. Fig. 5-1 and Fig. 3-1 show the schematic for the synthesis of SBA-15 and the impregnated metal catalyst.

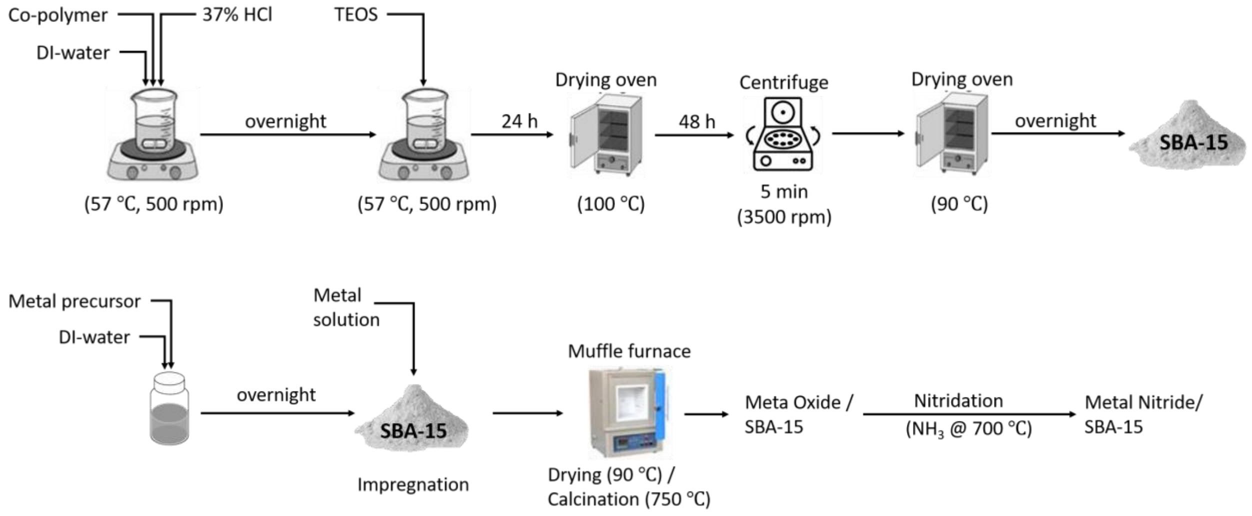

Fig. 3-1: Schematic of catalyst synthesis. Top row for the ordered mesoporous SBA-15 support and the bottom row for metal impregnation.

Table 3-2: Metal loadings of total 4 wt% for catalysts with different Mo:W molar ratios.

Catalyst	**Total metal [mmol/g_{Cat}]**	**Mo:W [mol/mol]**
Mo	0.417	-
5:1	0.362	5.0
4:1	0.352	4.0
2:1	0.319	2.0
1:1	0.286	1.0
1:2	0.259	0.5
1:5	0.236	0.2
W	0.218	-

The metal and mixed-metal nitride catalysts were prepared in-situ and directly prior to the activation experiments as described earlier for the gallium samples and depicted in Fig. 3-2. The parent samples (metal oxides) were purged with Ar (99.999%, Linde) for 1 h at room temperature to remove air, then dried at 90 °C (5 °C min^{-1}) for 0.5 h and then the temperature was increased to 700 °C (5 °C min^{-1}). Once the temperature stabilized, 50 vol% NH_3 (99.99%, Linde) with the balance Ar (4 ml_N min^{-1} NH_3 and 4 ml_N min^{-1} Ar) was introduced onto the sample for 3.5 h followed by 0.5 of purging with Ar to remove any residual ammonia in the lines before starting activation at 700 °C.

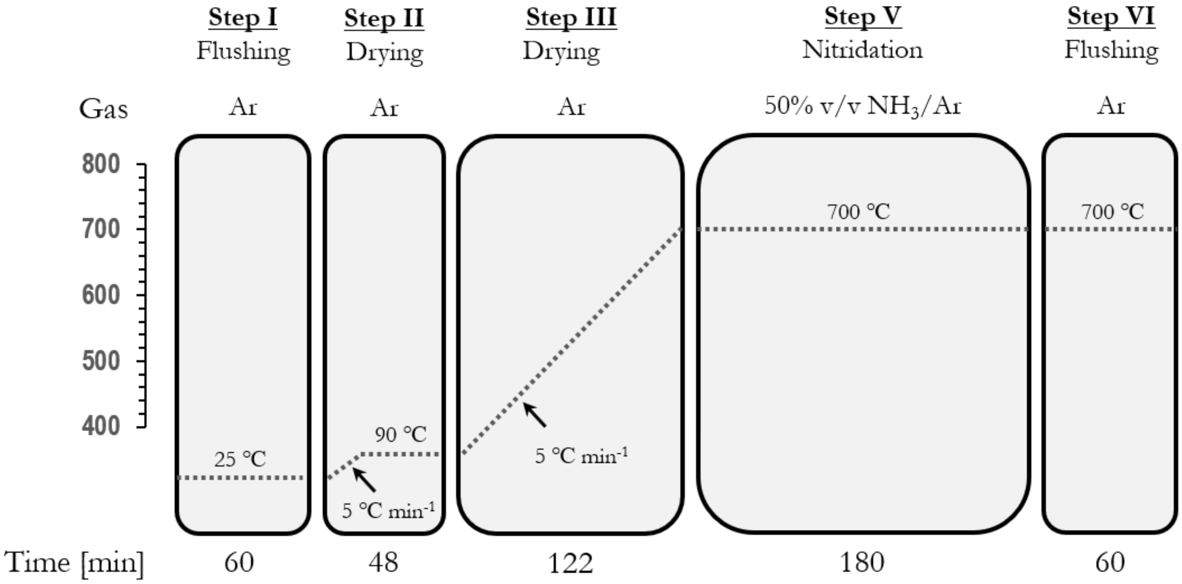

Fig. 3-2: Temperature/time scheme for the preparation of the metal nitrides catalyst supported on SBA-15 at 1 bar.

3.1.3 Catalyst nomenclature

The catalysts prepared where all supported on SBA-15 with a total loading of 4 wt% metal. The SBA-15 was prepared in two batches, first batch (B1) impregnated with Mo and W single metal catalysts and second batch (B2) impregnated with mixed metal catalysts. The supported synthesized oxide catalysts were named Mo/SBA-15 and W/SBA-15 for single metals. The mixed metal catalysts supported on SBA-15 were named: MoW(5:1)/SBA-15, MoW(4:1)/SBA-15, MoW(2:1)/SBA-15, MoW(1:1)/SBA-15, MoW(1:2)/SBA-15, MoW(1:5)/ SBA-15. Similarly, single metal nitride catalyst were named MoN/SBA-15 and WN/SBA-15. The mixed-metal nitride catalysts were named: MoWN(5:1)/SBA-15, MoW(4:1)/SBA-15, MoWN(2:1)/SBA-15, MoWN(1:1)/SBA-15, MoWN(1:2)/ SBA-15, MoWN(1:5)/SBA-15. In detail, MoN refers to 4 wt% molybdenum metal loaded catalyst on SBA-15 nitridated for 3 h at 700 °C. Similarly, MoWN(5:1)/SBA-15 refers to catalyst with total metal loading of 4 wt% and atomic ratio of 5 Mo and 1 W supported on SBA-15 that was nitridated for 3 h under 50 vol% NH_3 (4 ml_N min^{-1} NH_3 and 4 ml_N min^{-1} Ar) at 700 °C.

3.2 Catalyst characterization

3.2.1 Nitrogen adsorption/desorption measurements

Nitrogen adsorption/desorption measurements (-196 °C) were conducted using Gemini® VII 2390 surface analyzers to determine the total surface area, pore size distribution, pore volume, and pore width of the samples. Prior to every analysis run, the samples were degassed and dried at 90 °C for 0.5 h followed by 4.5 h at 250 °C (total 5 h) under helium gas flow (He, 99.999%, Praxair) in a degasser (Micromeritics FlowPrep 60). The pore size distribution was determined via the Barret-Joyner-Halenda (BJH) model using the desorption data, whereas the pore volume was determined based on the amount of adsorbed N_2 at $p/p_0 = 0.97$. The total Brunauer-Emmett-Teller (BET) surface area was calculated based on BET measurements in the pressure range 0.05 – 0.3 p/p_0.

3.2.2 X-ray diffraction (XRD)

X-ray powder diffractograms were recorded on a Bruker D8 Discovery X-Ray diffractometer with a CuKα (λ=1.54056 Å) radiation source. The measurements were carried out at a tube voltage of 40 kV and a tube current of 20 mA, from the 2θ angle of 10° to 110° and a scan rate of 5 °C min^{-1}. The diffractograms were identified using the powder diffraction file (PDF) reference standards.

3.2.3 Scanning electron microscopy and energy-dispersive X-ray spectroscopy (SEM-EDS)

Ultra-high-resolution field emission scanning electron microscopy (Hitachi, Cold FE SU-8000 SEM) with an accelerating voltage of 5.0 kV and emission current of 10 μA was used for the morphological characterization of the SBA-15 before and after the deposition of Mo and W oxides and nitrides. Energy-dispersive X-ray spectroscopy (EDS) was used to investigate the elemental composition and mapping of the samples. The samples were mounted on copper tape prior to imaging.

3.2.4 X-ray photoelectron spectroscopy (XPS)

Element identification and their chemical state were investigated by X-ray photoelectron spectroscopy (Thermo-Scientific, K-alpha XPS apparatus) with an Al Kα source, micro-focused monochromator, and spot size of 400 μm. The powder samples were mounted on copper tape and then degassed in a vacuum desiccator overnight and then mounted on copper tape for the XPS test. The flood gun was turned on to avoid the charging effect during data acquisition. The obtained spectra were analyzed using the Avantage software after Shirley background subtraction.

3.2.5 Temperature-programmed oxidation (TPO)

Temperature programmed oxidation (TPO) was carried out on the spent catalysts using a Netzsch F1 Libra thermogravimetric analyzer (TGA) to measure the coke content. Approximately 20 mg of the spent catalyst was loaded into the TGA and heated to 900 °C at a heating rate of 1 °C min^{-1} in the presence of air and held at 900 °C for 30 min while measuring the weight changes

3.3 Experimental setup and procedures

3.3.1 Catalytic activity measurement

The metal oxide and mixed-metal oxide catalysts were reduced with 50 vol% H_2 (99.999%, MEGS) with balance Ar (4 ml_N min^{-1} H_2 and 4 ml_N min^{-1} Ar) for 2 h to form corresponding metal catalysts.

The nitride catalysts were reduced under ammonia flow (as explained in the methodology section) to form the metal and mixed-nitride catalysts. The catalyst pre-treatments (i.e., reduction or nitridation) and catalytic performance were conducted in a vertical packed bed reactor at 700 °C and 1 bar_{abs}. A quartz tube (9 mm OD×7mm ID×375mm long) with a 15–40 µ frit at one end was used as the reactor inside a vertical tube furnace (Mellen Company). Vögtlin red-y smart mass flow controller (± 0.3% accuracy, Switzerland, CH_4 MFC, NH_3 MFC, and Ar MFC in Fig. 3-3) was used to control the inlet flow of CH_4 (99.999%, Linde), Ar (99.999%, Linde), H_2 (99.999%, MEGS) and NH_3 (99.99%, Linde). Due to the volatile nature of the organic components as products (i.e., C_6H_6, C_7H_8, $C_{10}H_8$), the transfer lines were heated to approximately 200 ºC to avoid any condensation (shown in red, Fig. 3-3).

A mass spectrometer (Hiden Analytical, HPR-20) was used to analyze the outlet stream. The instrument was set to acquire mass spectra 0 to 150 atomic mass units (amu). The MS was used in Faraday mode that is capable of measuring concentration as low as 150 ppm. The MS was calibrated for hydrogen (H_2, 2 amu), methane (CH_4, 15 amu), ethylene (C_2H_4, 27 amu), propylene (C_3H_6, 42 amu), argon (Ar, 40 amu), carbon dioxide (CO_2, 44 amu), benzene (C_6H_6, 78 amu), toluene (C_7H_8, 91 amu) and naphthalene ($C_{10}H_8$, 128 amu) using standard gases and liquid component mixtures. Argon gas was used as an internal standard with a calibration factor of 1. The calibration factor for all components was calculated based on their intensity ratio as follows:

$$CF_i = \frac{C_i}{C_{Ar}} \frac{I_{Ar}}{I_i} \qquad 3-1$$

Where the intensities were measured in torr units (I, unit torr [torr]), and the concentration (C) refers to the concentration of the gas in the calibration mixture in vol%. By doing so the calibration factors for the expected components in the outlet stream were acquired using calibration gas cylinders (primary standards with ± 1% accuracy). The liquid calibration mixture was injected into the heated line (120−150 °C) using a syringe pump (New Era NE-1000).

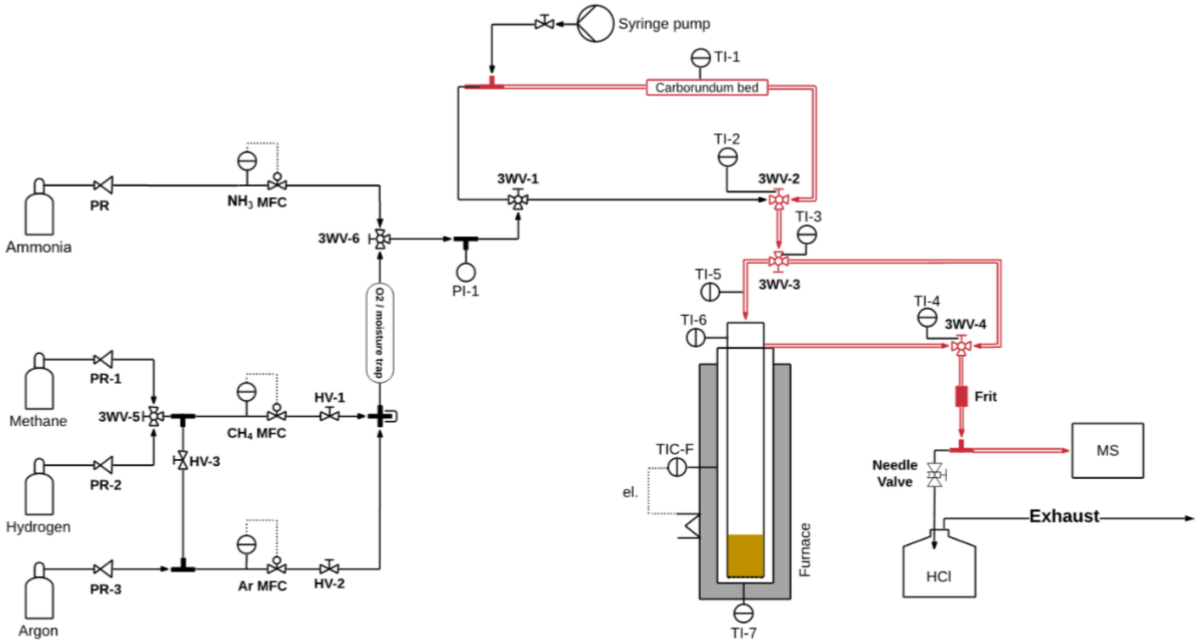

Fig. 3-3: Simplified P&ID of the packed bed reactor setup. (PR pressure regulator; MFC = mass flow controller; HV = hand vale; PI = pressure indicator; TI = temperature indicator; TIC = temperature indicator control; 3WV = 3-way valve).

To ensure evaporation of the volatile components, a vertically oriented carborundum was placed inline where the cold liquid mixture was injected. To have an oxygen-free system, an oxygen/moisture trap (Supelpure®-O, Sigma Aldrich) was placed in line with the inlet gas flow to the reactor.

The temperature of the reactor was controlled using a K-type thermocouple (TIC-F) that also measured the furnace temperature. A secondary thermocouple (TI-7) was placed at a different location in the furnace as backup. The internal catalyst bed temperature was verified by using a temporary thermocouple immersed in the catalyst bed. This resulted in a maximum difference of 2 °C between the furnace thermocouple and the catalyst bed thermocouple (temporary) at 700 °C (Fig. 3-4 inset), that was within the error range (± 0.75%, i.e., ± 5 °C at 700 °C) of the K-type thermocouple used and is considered acceptable. Before every step in the tests, a 30 min stabilization was time added to ensure the bed has reached the setpoint temperature and the temperature controller had enough time to stabilize as shown in Fig. 3-4.

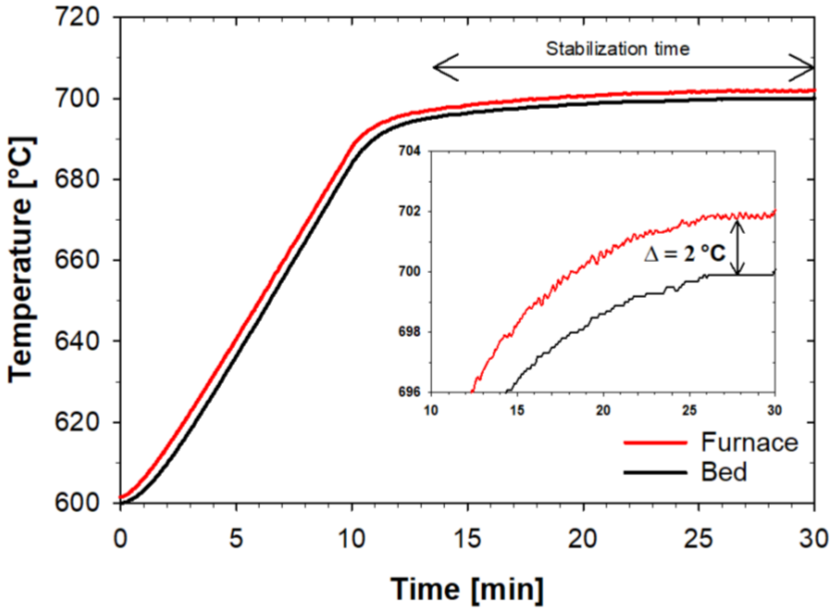

Fig. 3-4: Catalyst bed vs. furnace temperature.

Approximately 200 mg of the metal oxide or mixed metal oxide catalysts were loaded into the fixed bed quartz reactor. Based on Mo:W ratio the bed height varied between 16−22 mm. Prior to heating and activity measurement, the catalyst was purged with Ar (20 ml_N min^{-1}) for 1 h, then heated to 700 °C at a rate of 5 °C min^{-1}, and then the metal oxides were either (1) reduced with H_2 for 1 h to form metals and mixed metals or (2) nitridated with NH_3 for 3 h to form the corresponding metal and mixed metal nitride catalysts. After the nitridation, the gas lines were purged with Ar to remove any NH_3, N_2, H_2O, and N_2. After the catalyst treatment, 50 vol% CH_4 with balance Ar (4 ml_N min^{-1} NH_3 and 4 ml_N min^{-1} Ar) was added with a resulting CH_4-based gas hourly velocity (GHSV) of 1160 h^{-1}.

Detailed mass spectrum analysis was done on the outlet stream products to identify the components and determine methane conversion and determine the product flow rates as a function of time. Based on this, the MS was calibrated for hydrogen (H_2), methane (CH_4), ethylene (C_2H_4), propylene (C_3H_6), toluene (C_7H_8), and naphthalene ($C_{10}H_8$) to be quantified. Methane conversion [%] was calculated based on the gaseous carbon products (equation 3-2).

$$x_{CH_4} = \frac{\sum \nu_i \cdot \dot{n}_i}{\dot{n}_{CH_4,in}} \cdot 100 \qquad \text{3-2}$$

Where n_i denotes the molar flow of the i^{th} component, and vi is the number of carbon atoms in the i^{th} species in the product stream (i.e., C_2H_4, C_3H_6, CO_2, C_7H_8, and $C_{10}H_8$). The denominator is the inlet molar flow rate of CH_4 in the feed. The conversion represents the % C converted to hydrocarbon and not coke. The results reported were within 5% of C and H of the elemental balance.

3.3.2 Diffuse reflectance infrared Fourier transform spectroscopy (DRIFTS)

Diffuse reflectance infrared Fourier transform spectroscopy (DRIFTS) spectra technique was used to observe and determine adsorbed surface species and reaction intermediates over unsupported (GaN) and supported (GaN/SBA-15) gallium nitride catalysts in order to validate the proposed reaction mechanism published by our group [42]. However, DRIFTS was not performed on the Mo and W catalysts for the mechanistic insight which remains outside the scope of this thesis. Spectra were recorded on a Thermo Scientific™ Nicolet™ iS50 FTIR Spectrometer equipped with a standard diffuse-reflectance attachment in the range of 400−6000 cm^{-1}, with a resolution of 4 cm^{-1} and 250 scans for signal accumulation and liquid nitrogen cooled MCT detector. For in-situ measurement, a Harrick Praying Mantis™ high-temperature reaction chamber (with ZnSe window) was used, and the data was analyzed using OMNIC 9.11.706 software.

The DRIFTS experiment setup (Fig. 3-5) resembled closely the actual fixed-bed reactor setup used for activation experiments as shown in Fig. 3-3. The gas flow configuration in the reaction chamber was set to mimic the pack bed configuration with the gas entering from the top and exiting through the bottom of the sample cup. Similar to the setup in Fig. 3-3, the transfer lines were heated using heat tapes to avoid any condensation of the products. The chamber temperature was controlled with a thermocouple referred to as TIC-1 in Fig. 3-5, which was placed underneath the sample in the reaction chamber. The gas flows were controlled using the same MFC's discussed in section 3.3.1.

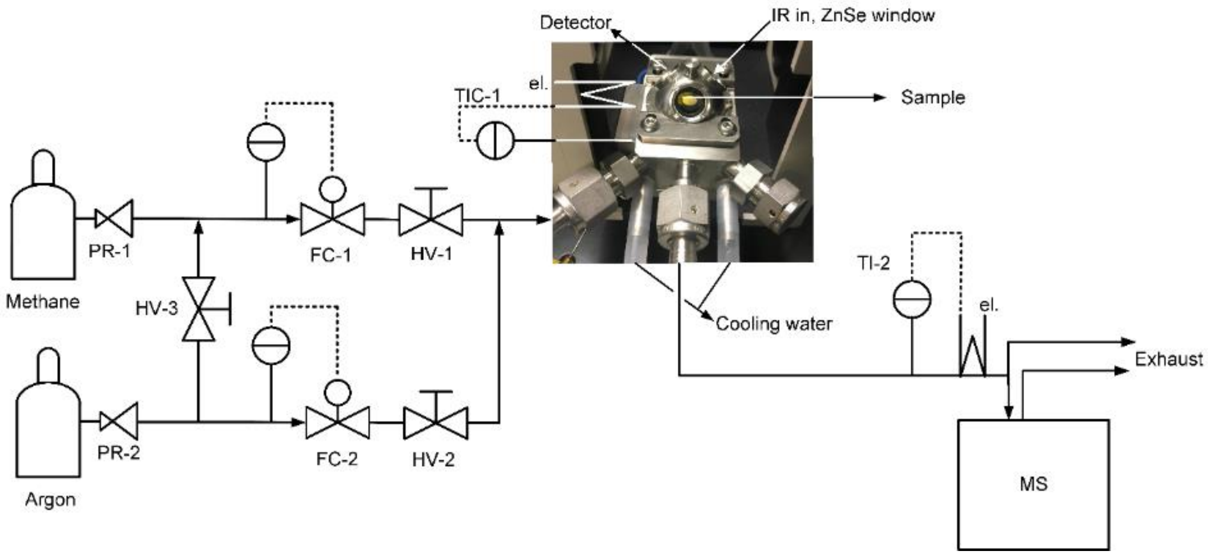

Fig. 3-5: Diffuse reflectance infrared Fourier transform spectroscopy (DRIFTS) setup for direct non-oxidative methane activation [31].

In the DRIFTS experiment, sample preparation is necessary to get optimized spectra. For the analysis, the catalysts were diluted with potassium bromide (KBr, Infrared grade, Fisher Chemical), which was crushed (< 20 μm), dried overnight at 150 °C, and stored inside a desiccator. Around 9.5 mg of supported GaN/SBA15 (2.5 mg of unsupported GaN) was mixed thoroughly with 14 mg (17.5 mg KBr for GaN) of dried KBr.

The catalyst-KBr sample was placed on quartz wool (previously dried overnight at 150 °C, cooled, and stored inside the desiccator) inside the high-temperature reaction chamber. The chamber was purged with Ar (10 $\mathrm{ml}_N\ \mathrm{min}^{-1}$) for 1 h at room temperature and then heated under Ar (10 $\mathrm{ml}_N\ \mathrm{min}^{-1}$) to 650 °C (10 °C min^{-1}) to remove moisture and adsorbed CO_2. It was then cooled down (or heated) under Ar (10 $\mathrm{ml}_N\ \mathrm{min}^{-1}$) to the initial temperature of the analysis and the background was collected at this temperature. Two studies were carried out after the purging and drying, (1) isothermal DRIFTS at 700 °C, and (2) temperature-programmed DRIFTS (TP−DRIFTS) from 400−700 °C. In the second approach, the experiment was started at 400 °C. The CH_4 flow rate was set to 2.0 $\mathrm{ml}_N\ \mathrm{min}^{-1}$ and the Ar flow rate to 0.5 $\mathrm{ml}_N\ \mathrm{min}^{-1}$. After 30 min, CH_4 was stopped, and the Ar flow rate was gradually increased to 15 $\mathrm{ml}_N\ \mathrm{min}^{-1}$. The Ar flow was held for about 25 min to assure that CH_4 has been removed completely (confirmed via MS and the IR spectra). After that, the temperature was increased by 50 °C increments (20 °C min^{-1} heating rate) under Ar atmosphere. Around 10 min of stabilization time was given before starting CH_4 again. During this whole time (starting from the background collection), the IR spectra were collected continuously. To confirm that the surface intermediates were forming on the catalysts, the support (SBA−15) and nitridated support (N−SBA−15) were also tested, at 700 °C with 80% CH_4 in Ar (2.0 $\mathrm{ml}_N\ \mathrm{min}^{-1}$ CH_4 and 0.5 $\mathrm{ml}_N\ \mathrm{min}^{-1}$ Ar).

To compare the DRIFTS conditions to the actual reactor in the lab, in terms of loading, the total GaN/SBA-15 catalyst mixed KBr was 1.5 mg compared to 19 mg in the actual reactor. This resulted in a lower bed height and thus residence time which was <0.5 s for DRIFTS setup and <2 s in the fixed bed reactor.

Chapter 4

4 Gallium nitride (GaN)

The first non-oxidative methane activation experiments were conducted over gallium nitride catalyst in collaboration with my former colleague Dr. Kanchan Dutta. This served as part of my training (i.e., catalyst synthesis and characterization) in the lab. The work on Ga catalyst was done as collaborative work. The first part of this section summarizes the work done on DRIFTS experiments elucidating the surface species and reaction intermediates over gallium nitride. The second part provides a summary of the catalyst regeneration work on the spent gallium nitride catalyst utilizing thermogravimetric analysis.

4.1 Diffuse reflectance infrared Fourier transform spectroscopy (DRIFTS)

DRIFTS was used for the first time in our group to validate and elucidate the surface species and intermediates at the reaction conditions (700 °C and 1 bar) for the reaction converting CH_4 to ethylene over GaN catalysts. I was responsible for setting up the instrument and carrying out the DRIFTS experiments. Before running the experiments, several questions needed to be answered which includes dilution degree with KBr for optimum signal, masking effect of CH_4 peaks, and the influence of the supports. This involved several trials and errors to find the working parameters for our experiment; an SOP was drafted for future use of the instrument with experimental procedure and conditions.

4.1.1 The masking effect of CH_4 on the spectra for the adsorbed species

When collecting spectra during the methane activation experiments, two dominant peaks at 3015 cm^{-1} and 1305 cm^{-1} (brown spectra in Fig. **4-1**) were observed that correspond to the νC−H and δC−H bands of CH_4, which masked the spectra of any adsorbed species of interest [44]. To eliminate the masking effect of CH_4, the sample was purged after every experiment to remove the methane from the cell along with the physisorbed species. The resulting signal is illustrated by the pink spectra for GaN/SBA-15 (Fig. **4-1**), which are described in detail in later sections.

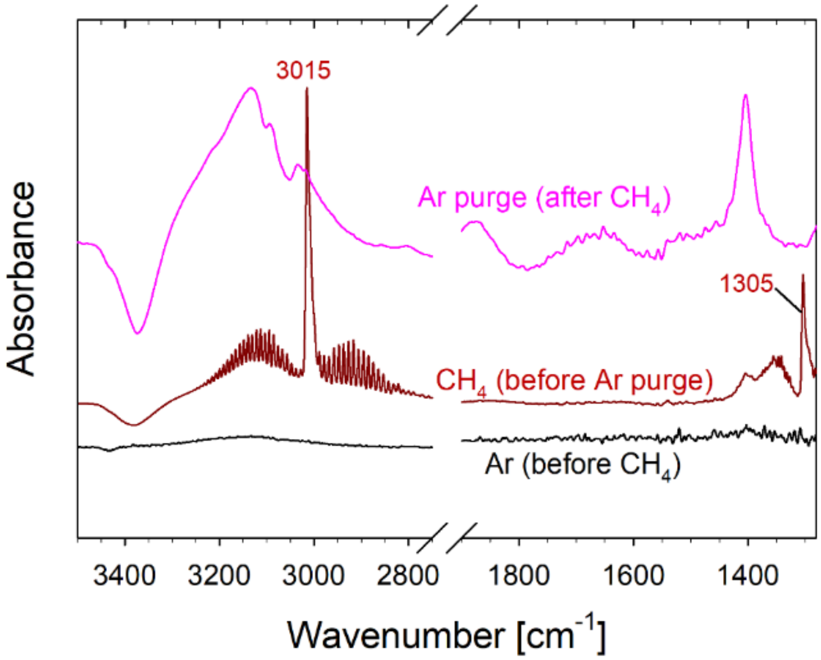

Fig. 4-1: Masking effect of CH_4 on the DRIFT spectra for GaN/SBA15 at 700 °C (80% CH_4 in Ar with 2.0 ml_N min^{-1} CH_4). All spectra were corrected for the background spectrum under Ar at 700 °C [31].

4.1.2 Effect of dilution with KBr

Besides the masking effect, the dilution of the solid sample is crucial in getting optimum spectra in the DRIFTS experiment. When pure samples were used for the experiments, the spectra did not show any characteristic peaks (orange spectra in Fig. 4-2). To find the optimum dilution degree required, the supported GaN/SBA-15 and unsupported GaN samples were tested with different dilution degrees with KBr to see the effect of dilution as illustrated in Fig. 4-2. In the case of supported GaN/SBA-15, characteristic peaks were observed, however, with a low signal-to-noise ratio at low wavenumbers (<2000 cm^{-1}). Dilution of the samples to 40 wt% in KBr, resulted in clearer signals and revealed peaks that would not be seen before, peak at 1400 cm^{-1} that was common to both supported GaN/SBA-15 and unsupported GaN. Similarly, for the unsupported catalyst, dilution of 12.5 wt% in KBr resulted in a good signal-to-noise ratio. As a result, for all experiments, the supported samples were diluted to 40 wt% and unsupported to 12.5 wt% in KBr. The peaks associate with CH_4 adsorption and reaction will be explained in detail in subsequent sections.

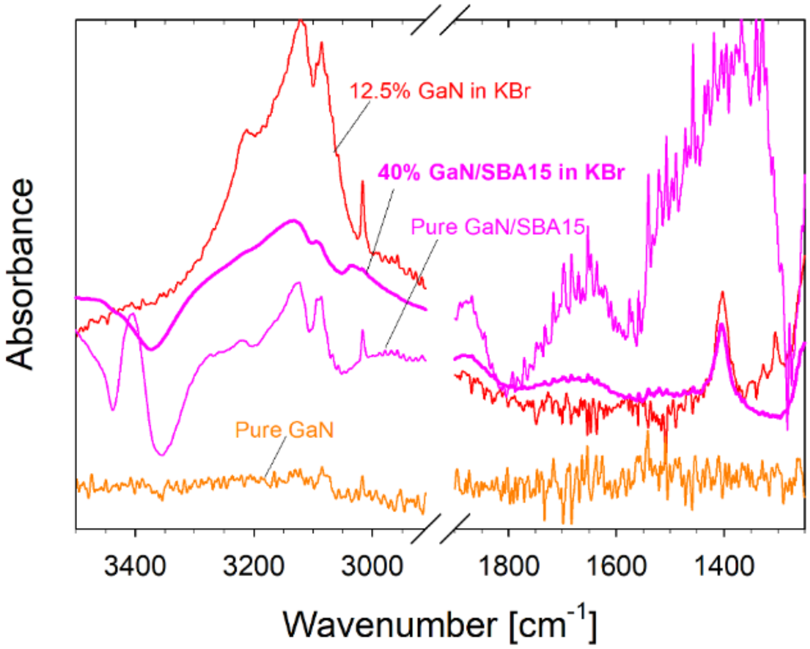

Fig. 4-2: Effect of dilution on the DRIFT spectra for the methane activation catalysts. The spectra were collected during Ar purge (15 ml$_N$ min^{-1}) after 1 h CH_4 activation at 700 °C (80% CH_4, 2.0 ml$_N$ min$_{-1}$ CH_4). All spectra are corrected for the background spectrum under Ar at 700 °C [31].

4.1.3 Influence of support

Methane activation over SBA-15 and N-SBA-15 (nitridated support) did not exhibit any peaks corresponding to carbon adsorbed species such as the CH_3, C–H, aromatics, or alkene C=C bonds which were visible during CH_4 activation on GaN and GaN/SBA-15 catalyst (Fig. 4-3). This confirmed that the support was mostly inert towards the non-oxidative methane activation. Upon nitridation of the support, a broad peak at 3400 cm^{-1} was observed corresponding to the N-H bond, that is formed during the nitridation. Also, the SBA-15 and N-SBA-15 support had peaks between 1350 cm^{-1} and 1400 cm^{-1} due to their inorganic structure which were absent in Ga loaded SBA-15 sample.

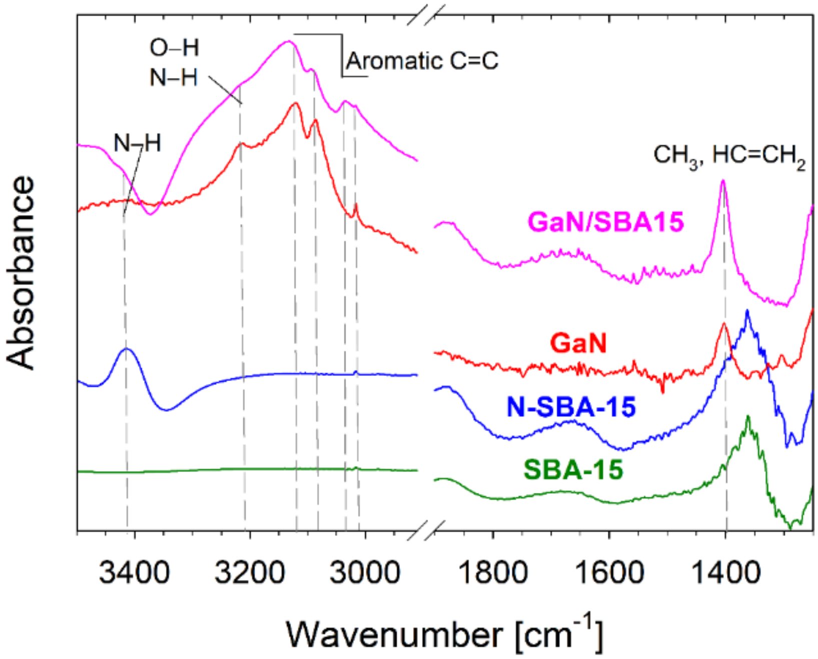

Fig. 4-3: Comparison of the DRIFT spectra for the supports (SBA−15 and N−SBA−15) with the supported GaN/SBA15 and the unsupported GaN. The spectra were collected during Ar purge (0.5 h at 15 ml_N min^{-1}) after 1 h CH_4 activation at 700 °C (80% CH_4 in Ar with 2.0 ml_N min^{-1} CH_4). All spectra were corrected for the background spectrum under Ar at 700 °C [31].

4.1.4 Adsorbed species observed over GaN and GaN/SBA15

The peaks observed in the DRIFTS spectra are summarized for unsupported GaN and supported GaN/SBA-15 collected after 1 h activation with CH_4, purging with Ar, and cool down (Fig. 4-4). Characteristic peaks for both GaN and GaN/SBA-15 showed up at around the same wavenumbers (± 15 cm^{-1}). The results obtained agreed with the DFT proposed intermediates appearing at the surface of the catalyst, (Ga−CH_3, CH_2), aromatic species, and vinylidene ($H_2C=CH-$) [42]. The peak at 1402 cm^{-1} is due to the symmetric bending in CH_3. The bands at 1500–1400 cm^{-1} (deformation, medium intensity) and 1380–1160 cm^{-1} (wagging, medium intensity) are attributed to the methylene (>CH_2)

peaks. The peaks for alkenes (isolated C=C, vinyl), appear between 1600–1740 cm^{-1} with weak–strong intensities. The vinyl hydrocarbon peaks are shown by the medium-strong peak observed at 1400 cm^{-1} attributed to the in-plane CH_2 deformation vibrations. The band 3105−3000 cm^{-1} is attributed to aromatic (sp^2) =C−H stretching, with medium intensity. The medium intensity band at 1470−1430 cm^{-1} is also due to the −C=C− stretching vibrations. The in-plane bending of C–H in aromatics is attributed to the peak around 1240 cm^{-1} [45].

In the second part, the temperature-programmed (TP-DRIFTS) were performed (refer to methodology chapter 3) to find the onset temperature at which the intermediate species started to show up and thus methane activation on the supported and unsupported GaN catalyst. In the work by Li *et al.*, benzene was produced at 450 °C [41], however, Dutta *et al.* did not observe any activity until 650 °C in the continuous flow reactor [46]. The spectra for the TP-DRIFTS are illustrated in Fig. 4-5 and Fig. 4-6. The onset for both catalysts was 450 °C. The results showed that olefinic species started showing up at 400 °C (Fig. 4-5) while aromatics species were observed at 450 °C (Fig. 4-5). The corresponding characteristic peaks and are discussed above. These results confirm the DFT work by Chaudhari *et al.* [42] and indicate that ethylene is formed first and then leads to benzene formation [42]. Peak assignment for adsorbed species in Fig. 4-5 and Fig. 4-6 are summarized in Table 4-1.

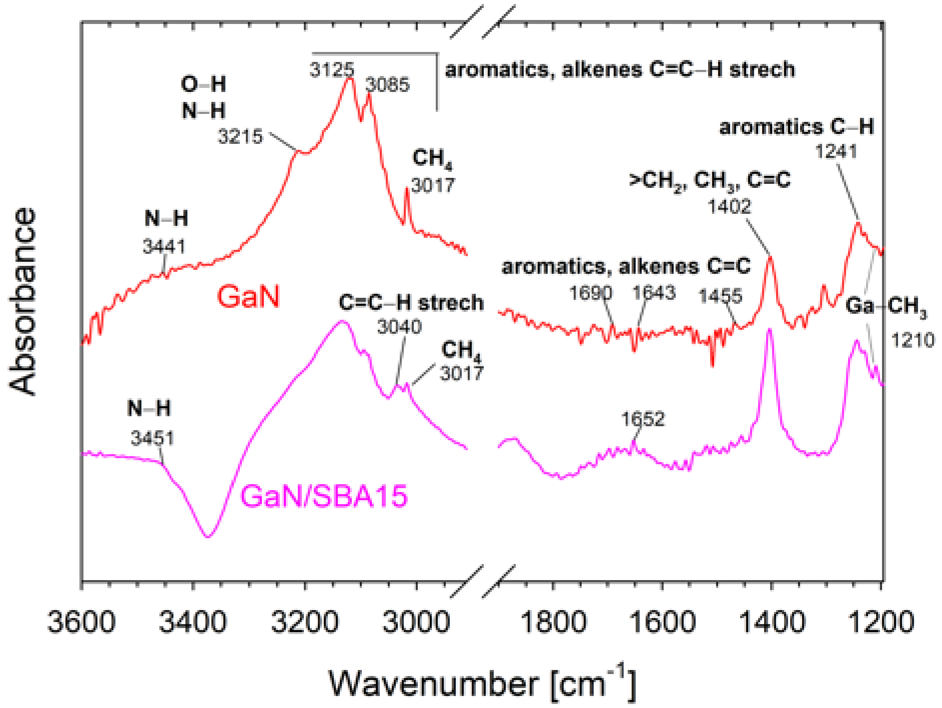

Fig. 4-4: DRIFT spectra for unsupported GaN and supported GaN/SBA15 collected under Ar purge, after 1 h exposure to CH_4 (80% in Ar) at 700 °C. The peak corresponding to 3017 cm^{-1} is due to free CH_4. All spectra are corrected for the background spectrum under Ar at 700 °C [31].

Table 4-1: summary of observed species on supported GaN/SBA-15 and unsupported GaN [31].

Adsorbed species wavenumber [cm^{-1}]		**Assignment** [45]
GaN/SBA15	**GaN**	
2853, 2797	2926, 2887, 2791	C−H stretching alkane, medium
3131, 3089, 3031	3104, 3070	Aromatic and alkene =C−H stretching, medium C−H stretching alkane, medium
–	3205	N−H stretch, O−H (silanol)
3451	3451 (broad shoulder)	N−H stretch
1402	1398	CH_2 in-plane deformation vibration
1513	1508	Methylene (>CH_2) deformation, medium
1692−1571	1701−1576	C=C stretching, weak to strong

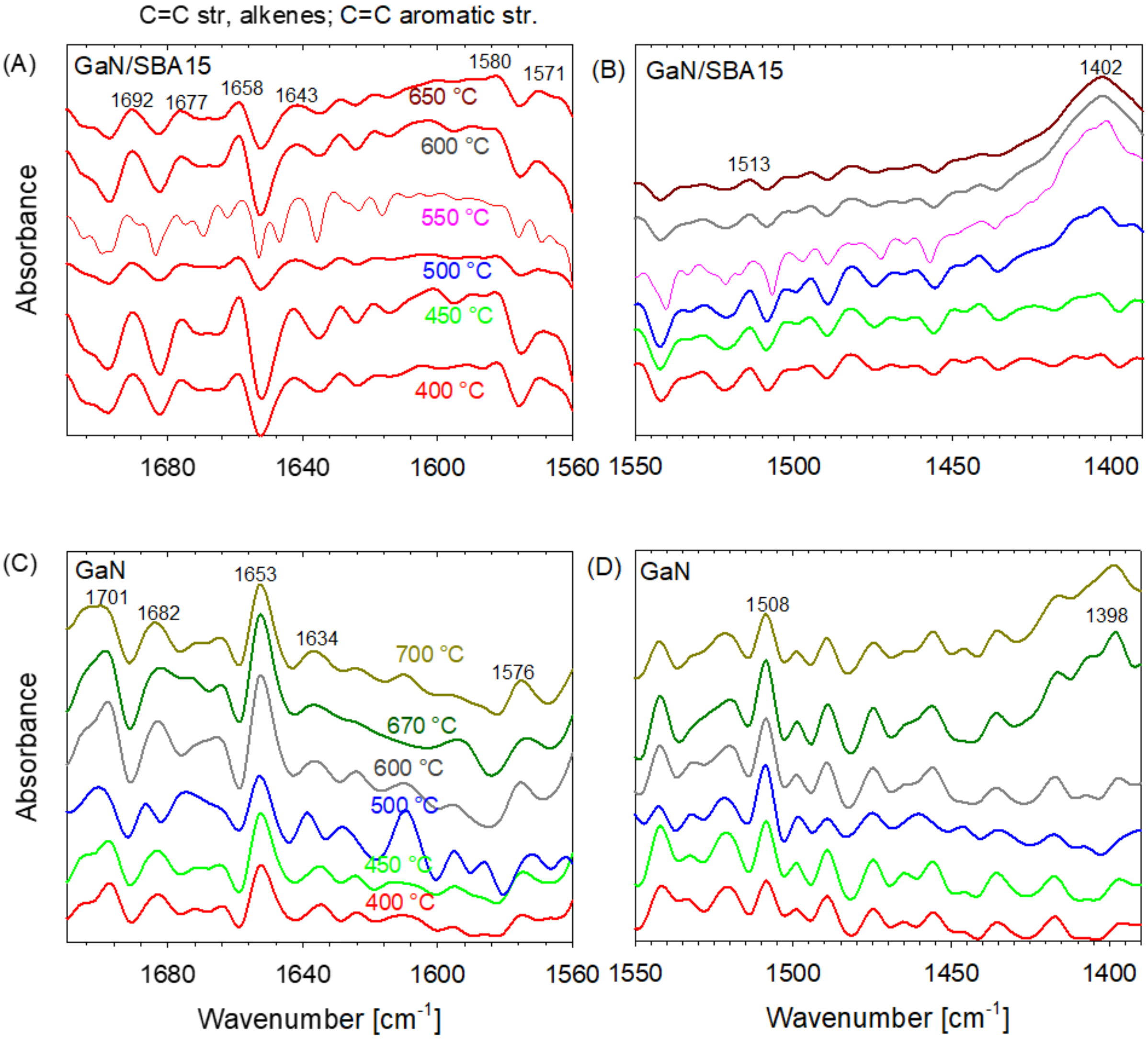

Fig. 4-5: Evolution of surface adsorbed species as a function of temperature on supported GaN/SBA15 (A) between 1600−1400 cm^{-1} and (B) between 1600−1400 cm^{-1}; for unsupported GaN (C) between 1600−1400 cm^{-1} and (D) between 1600−1400 cm^{-1}. The spectra were collected during Ar purge (15 ml_N min^{-1}) after 30 min CH_4 activation (80% CH_4 in Ar with 2.0 ml_N min^{-1} CH_4). All spectra are corrected for the background spectrum under Ar at 400 °C [31].

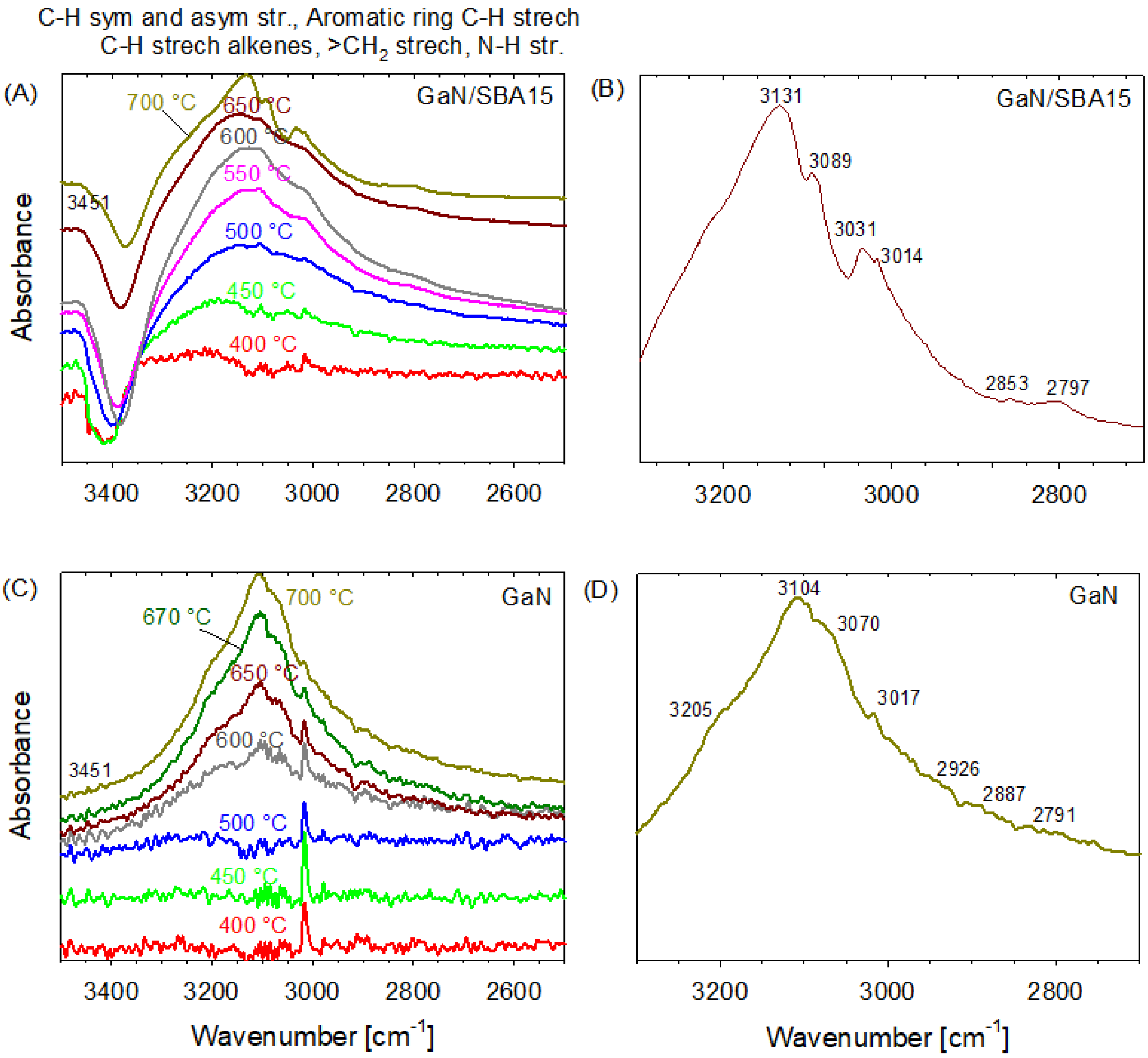

Fig. 4-6: Evolution of surface adsorbed species (between 3500−2500 cm^{-1}) over supported GaN/SBA15 (A) as a function of temperature and (B) at 700 °C; for unsupported GaN (C) as a function of temperature and (D) at 700 °C. The spectra were collected during Ar purge (15 ml$_N$ min^{-1}) after 30 min CH_4 activation (80% CH_4 in Ar with 2.0 ml$_N$ min^{-1} CH_4). All spectra are corrected for the background spectrum under Ar at 400 °C [31].

4.2 Catalyst regeneration GaN

Catalyst coking is considered the main issue in the non-oxidative methane activation at high temperatures mainly due to its role in catalyst deactivation. The regeneration capability and reusability of gallium nitride (GaN) catalysts for the direct non-oxidative methane activation with subsequent coupling to ethylene were studied. This work was published with me as the second author in the work by Dutta et al. [43]. My contribution to this work was performing the TGA experiments for the regeneration paper. In this work, the activity of the gallium nitride catalyst was assessed with multiple steps of catalyst activation, regeneration, and re-nitridation to extend the life of the catalyst.

Different regenerating agents were tested to find the best medium among air, H_2 and CO_2. Regeneration with H_2, and CO_2 was not desired since both required a high temperature of >800 °C to remove the coke. Furthermore, at this temperature GaN decompose into NH_3 and N_2, which resulted in metallic gallium remaining as a shiny metallic coating on the reactor wall. Moreover, high temperature causes the pores to collapse on the supported catalysts, reducing surface area as illustrated in (Fig. 5-1). The air was chosen as the preferred coke removal medium as the coke was burnt at temperatures of 450 to 500 °C for unsupported and 550 to 600 °C for supported GaN/SBA-15, which were much lower than the oxidation of the gallium nitride as indicated by the weight increase in Fig. 4-7.

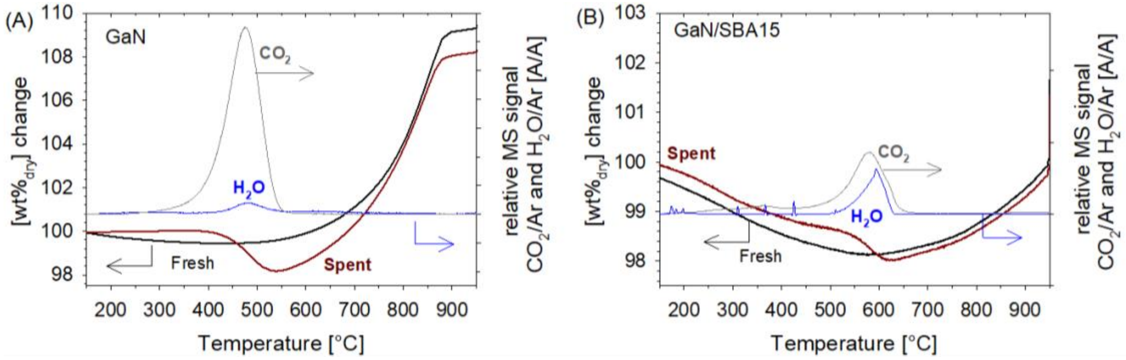

Fig. 4-7: TPO (MS and TGA) results for fresh and used (A) unsupported GaN and (B) supported GaN/SBA15 catalyst [43].

Fig. 4-8 illustrates the rate of carbon deposition on the surface of the catalyst as a function of time on stream for activation with methane at 700 °C. The 1st cycle had a slower rate and less total carbon deposition (2 to 4.5 μmol min^{-1} g_{Cat}^{-1} and 60 mg g_{Cat}^{-1}) compared to the 2nd and 3rd (80 mg g_{Cat}^{-1} and 80 mg g_{Cat}^{-1}). These values were 3–4 larger than what was achieved in the fixed bed reactor with 18 mg g_{Cat}^{-1}. This was expected as the gas flow pattern in the TGA, which was flowing above the sample rather than through the catalyst, introduces diffusion limitations. Approximately 4.25 h was sufficient to burn most of the coke but after extending it to a total of 12 h there was a slight weight increased (<0.13% of initial mass) indicative of surface gallium nitride oxidation. Regeneration with air results in the formation of Ga_2O_3 that produced CO_2, CO, and H_2O. The results showed that the re-nitridation after a regeneration cycle is crucial to maintain a constant ethylene yield over multiple regeneration steps.

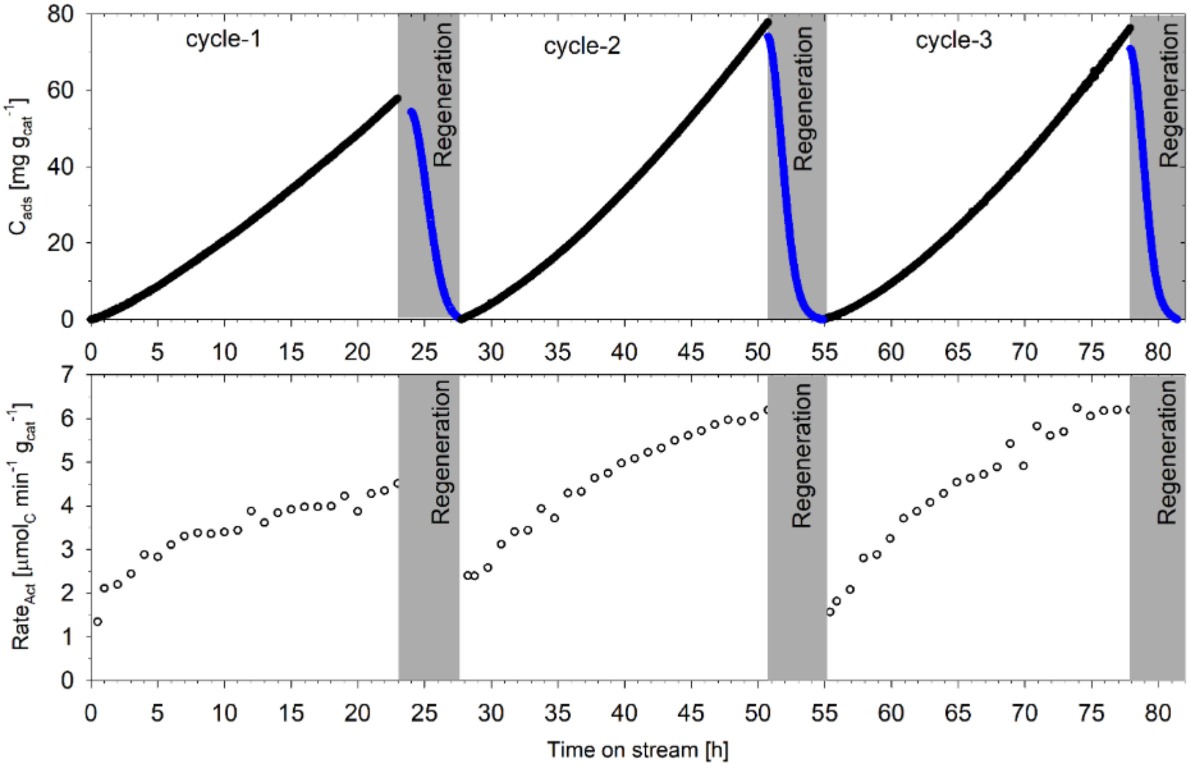

Fig. 4-8: TGA results for three methane activation and regeneration cycles. Activation: 700 °C with 20 mg GaN/SBA15, regeneration: air at 550 °C [43].

Chapter 5

5 MoW Mixed Metal Nitrides

5.1 Introduction

In this chapter the oxides and nitrides of molybdenum and tungsten single and mixed-metal catalyst with varying Mo:W ratios were prepared and characterized by means of N_2 adsorption, XRD, SEM, XPS, and TPO. All the samples used for characterization were either metal and mixed-metal oxides (i.e., they were not reduced with H_2 as done prior to activity tests) or metal and mixed-metal nitride catalysts. The effect of molar ratios on the selectivity and conversion were assessed on both reduced single and mixed-metal and their corresponding nitride catalysts for non-oxidative methane activation to olefins and aromatics. The results presented in this chapter will be presented at the 71st Canadian Chemical Engineering Conference (CCEC2021) in Montreal as well as submitted for publication in a peer-reviewed journal.

5.2 Characterization of fresh catalyst

5.2.1 N_2 adsorption/desorption

The Mo and W single metal catalysts were impregnated onto SBA-15 batch 1 (B1) and the mixed metal catalysts with varying Mo:W ratios were impregnated onto SBA-15 batch 2 (B2). All catalysts showed a unimodal pore size distribution at around 7.5 nm (Fig. 5-1). The synthesized SBA-15 supports were tested against temperature for different batches (Fig. 5-1). The results indicate the BET surface area of SBA-15 is strongly affected by the temperature (i.e., calcination, reduction, nitridation, activation or regeneration temperatures) and could decrease by 30% when exposed to 750 °C and by 48% reduction when exposed to 900 °C compared to the base 550 °C calcination temperature. As a result, the BET values at 750 °C were taken as baseline values for both B1 and B1 SBA-15 supports.

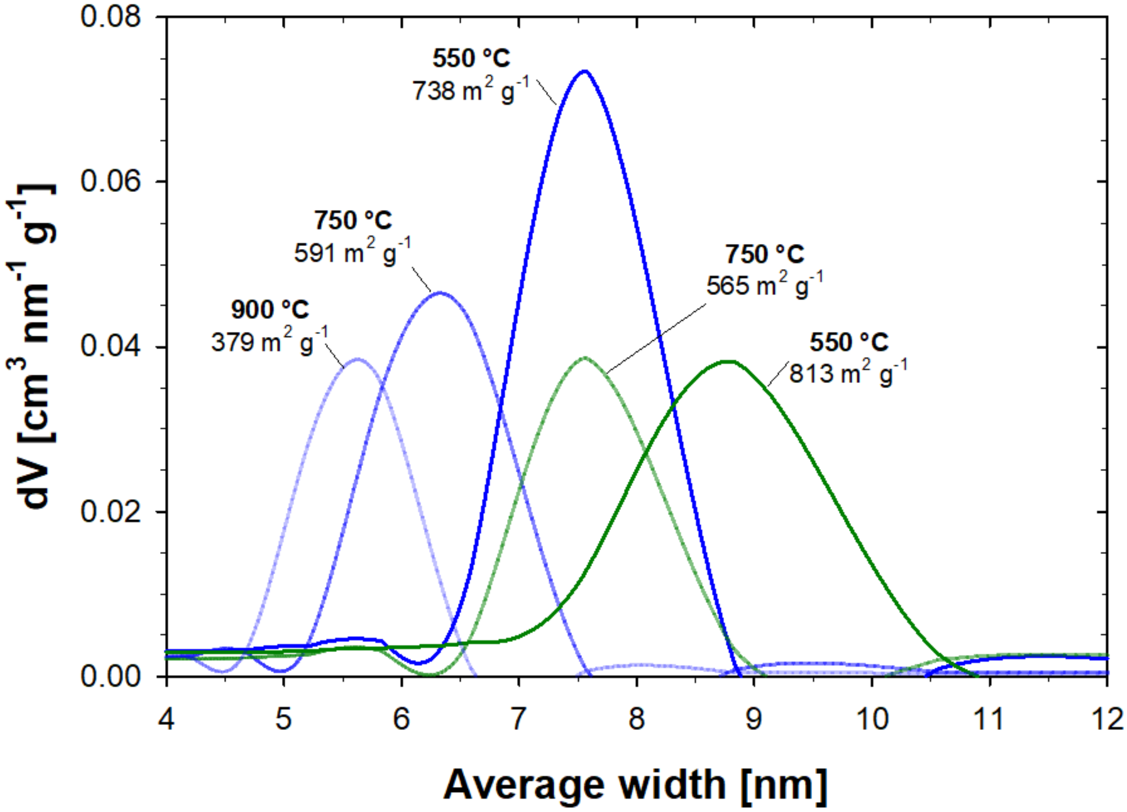

Fig. 5-1: Effect of calcination temperature on pore size distribution on SBA-15 prepared at different conditions. Green curves refer to batch 2 and blue curves refer to previous batch SBA-15 (see Table 3-1).

Metal deposition by means of impregnation reduced the BET surface area and pore volume of the impregnated SBA-15 samples significantly (Table 5-1). Moreover, samples with higher Mo content showed a greater contribution towards BET reduction. One reason could be due to the lower molar loading of W metal due to its higher molecular weight compared to Mo for a fixed amount of 4 wt% total loading. Also, this could be due to the formation of W agglomerates with tungsten containing catalysts as it was shown through SEM (Fig. 5-6). However, the average pore size stayed constant between different impregnated samples.

Table 5-1: Nitrogen adsorption and desorption results for supported metal catalysts.

Sample	S_{BET}[a] [$m^2\ g^{-1}$]	V_{Pore}[b] [$cm^3\ g^{-1}$]	D_{Pore}[c] [nm]	S_{BET}[a] Reduction [%]
SBA-15 (B1)	687	0.73	6.8	-
SBA-15/(B2)	565	0.61	7.0	-
Mo	268	0.55	11.4	61.0
5:1	349	0.52	8.6	38.2
2:1	415	0.52	7.6	26.5
1:1	398	0.49	7.3	29.5
1:2	440	0.52	7.3	22.1
1:5	486	0.55	7.2	14.0
W	561	0.63	7.0	18.3

[a] S_{BET} = BET total specific surface area obtained from adsorption data in the p/p^0 range from 0.06−0.2; all reported data are within ± 10 $m^2\ g^{-1}$ based on the repeated analysis.

[b] V_{Pore} = pore volume was obtained at $p/p^0 = 0.9$

[c] D_{Pore} = bimodal pore size distribution for all samples, calculated using the Barrett-Joyner-Halenda (BJH) method.

5.2.2 XRD

The XRD patterns of the fresh SBA-15, NSBA-15, and single and mixed-metal oxide and nitride samples are illustrated in Fig. 5-2A, while the spectra for the mixed-metal oxide and nitride samples with different Mo:W ratio is shown in Fig. 5-2B. The large diffraction peaks at around $2\theta = 16°$ and 19° were associated with SBA-15, which were observed in all the samples (PDF# 01-073-3462). However, these peaks ($2\theta = 16°$ and 19°) in the oxide samples containing tungsten revealed themselves as two distinct peaks with higher intensity at around $2\theta = 24°$, which is a characteristic peak for WO_3 (PDF# 00-020-1324).

MoN/SBA-15 and WN/SBA-15 nitride samples showed peaks corresponding to Mo_2N (PDF# 00-025-1366) and W_3N_4 (PDF# 04-019-2786) (Fig. 5-2a). The peaks for Mo_2N were also observed by

Cárdenas-Lizana *et al.* group for molybdenum oxide nitridation under N_2 and H_2 [47]. A low intensity peak at around 2θ = 16° for WN/SBA-15 sample also matches with the W_2N (PDF3 04-007-2211) reference, indicating the existence of multiple nitride species with different tungsten to nitrogen ratios. Furthermore, the oxide samples had a peak showing up around 2θ = 33° corresponding to MoO_3/SBA-15 and WO_3/SBA-15 which was absent for the nitride samples. This could be indicative of molybdenum and tungsten oxide peaks, which disappeared upon reduction into their corresponding nitrides. However, in the MoWN(1:5)/SBA-15 sample the oxide did not completely vanish, which could be due to either residual tungsten oxide that was not nitridated or converted to oxide during storage (Fig. 5-2B) The mixed metal oxides and nitrides showed multiple peaks, that could correspond to MoO_3 (PDF# 00-047-1081), WO_3 (PDF# 00-020-1324), and $Mo_5W_5O_{29}$ (PDF# 01-073-6268) for oxide catalysts and Mo_2N (PDF# 00-025-1366), W_3N_4 (PDF# 04-019-2786-), $MoWO_{2.4}N_{2.1}$ (PDF# 00-050-0134), $W_{0.2}Mo_{0.8}N_{0.51}$ (PDF# 04-019-8582) peaks were observed in the mixed nitride catalysts, summarized in Table 5-2.

Table 5-2: Crystallite size and observed species of the fresh metal and mixed-metal oxide samples.

Sample	Crystal size [nm]	Crystallite observed by XRD
Mo[1]	n/a	MoO_3
5:1	7.27	WO_3, MoO_3, $Mo_5W_5O_{29}$
2:1	9.58	WO_3, MoO_3, $Mo_5W_5O_{29}$
1:5	11.04	WO_3, MoO_3, $Mo_5W_5O_{29}$
W	11.93	WO_3
MoN	8.66	Mo_2N
5:1(N)	8.41	$MoWO_{2.4}N_{2.1}$, $W_{0.2}Mo_{0.8}N_{0.51}$, W_3N_4, Mo_2N
2:1(N)	8.43	$MoWO_{2.4}N_{2.1}$, $W_{0.2}Mo_{0.8}N_{0.51}$, W_3N_4, Mo_2N
1:5(N)	8.84	$MoWO_{2.4}N_{2.1}$, $W_{0.2}Mo_{0.8}N_{0.51}$, W_3N_4, Mo_2N
WN	19.51	W_3N_4, W_2N

[1] diffraction peak not large enough

The crystallite size of the samples ranged from 8 to 20 nm estimated using the Scherrer equation based on the strongest peak observed for every sample (Table 5-2). In the case of tungsten, reduction from oxide to nitride increased the crystallite size from 12 to 20 nm, however, the mixed metal and metals nitrides crystallite size were around 7–11 nm. It seems, that adding a small amount of Mo helps to disperse the W on the support and avoid sintering of W crystallites during the high temperature nitridation process. This effect was less pronounced for the mixed metal oxides. Summary of the crystallite size and the observed crystallites are presented in (Table 5-2).

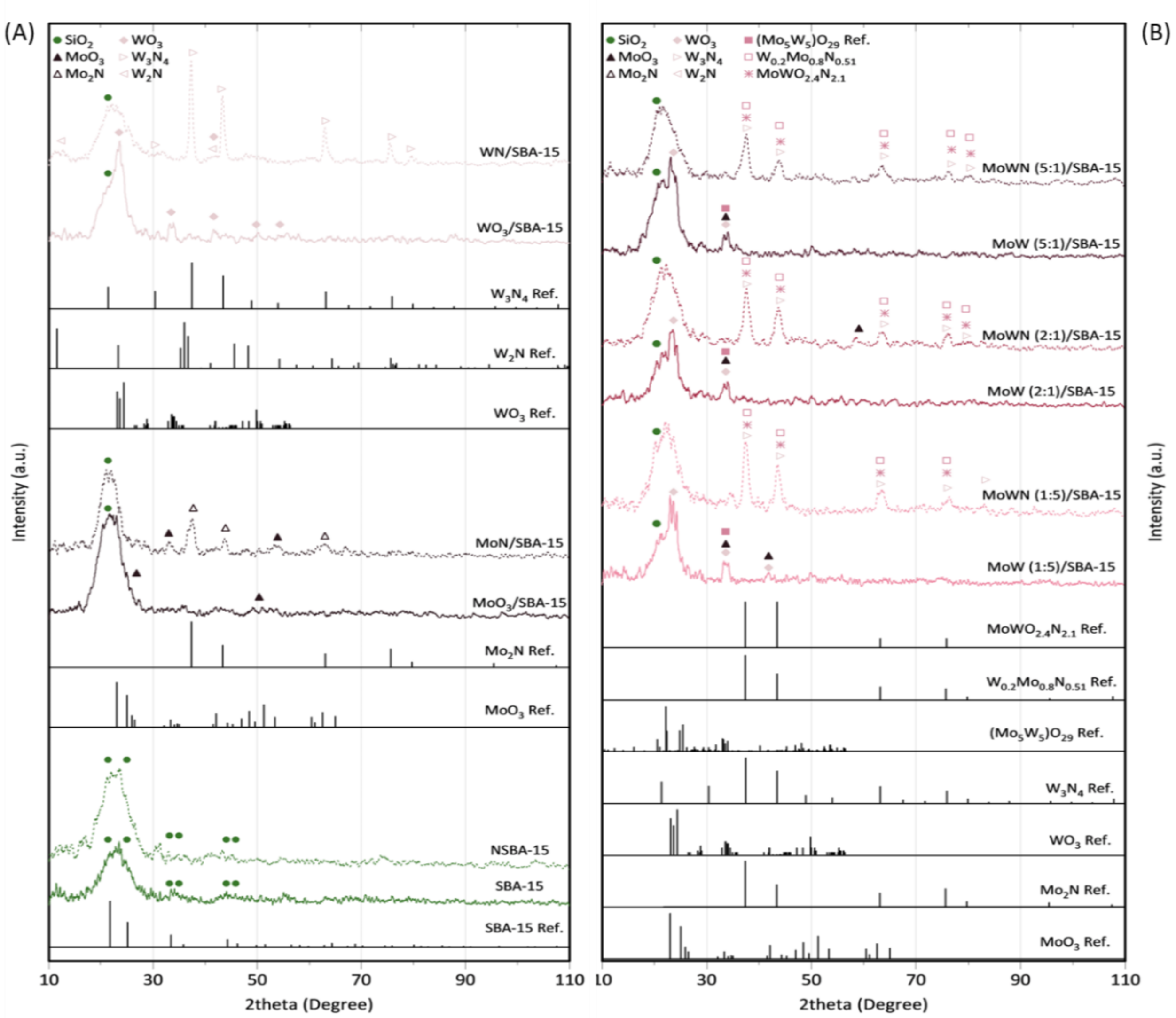

Fig. 5-2: XRD patterns of fresh SBA-15, NSBA-15, and (A) single and (B) mixed-metal oxide and nitrides catalysts.

5.2.3 SEM

The SEM images for SBA-15 calcined at 550 and 750 °C were taken to observe the morphology of the support (Fig. 5-3). SBA-15 showed rope-like domains in a relatively uniform size of ~1 μm, aggregated wheat-like macrostructures [48]. SBA-15 is reported to be thermally stable with SEM images showing a similar morphology [48]. However, the BET results indicate that exposure to high temperature affects the pore size and does decrease, as previously discussed (section 5.2.1, Fig. 5-1). In both samples there existed some areas where tube like structures of ordered mesoporous SBA-15 was not formed (Fig. 5-3B and D).

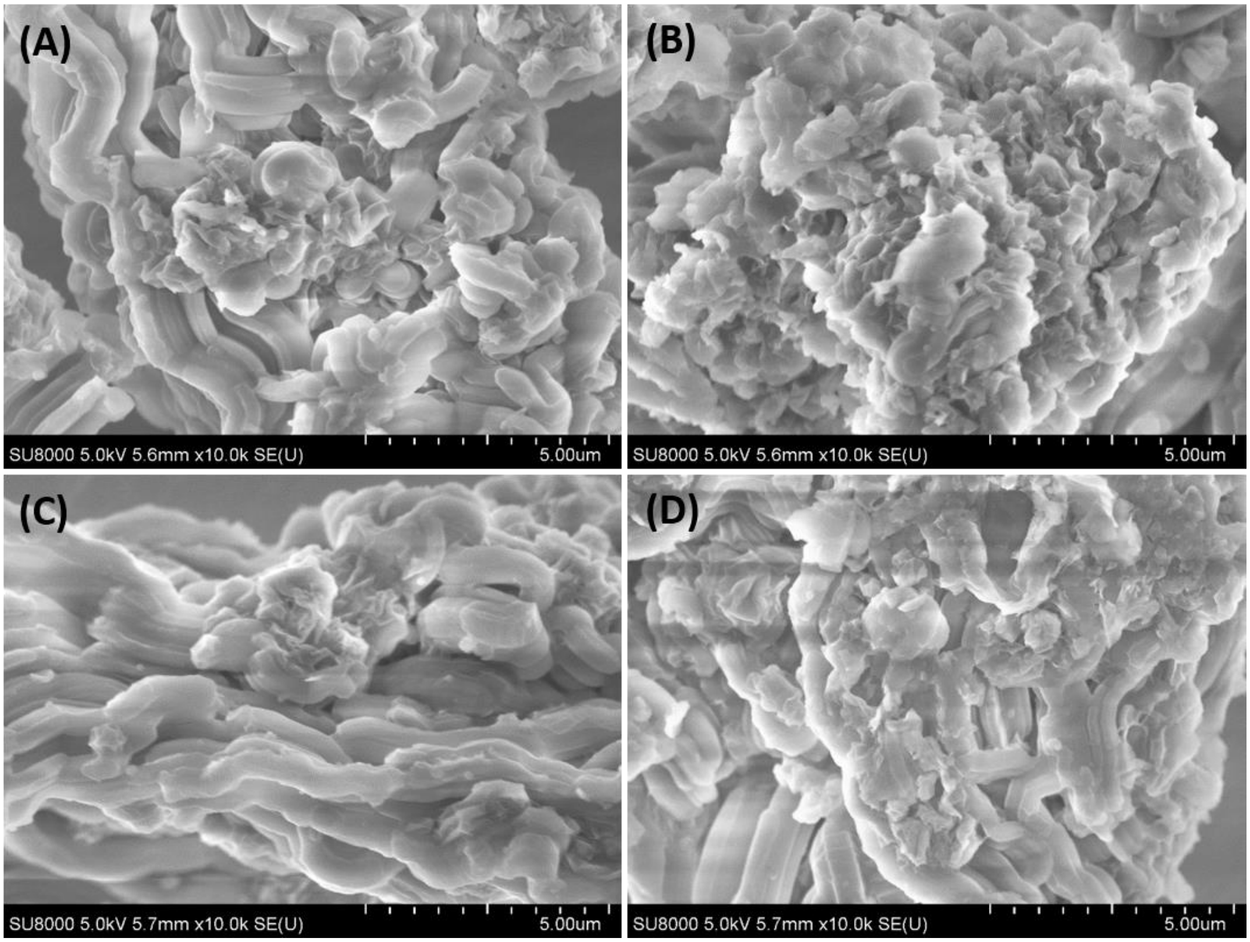

Fig. 5-3: SEM images of SBA-15 (A–B) calcined at 550 °C and (C–D) calcined at 750 °C.

The SEM images of fresh MoO_3/SBA-15 and MoN/SBA-15 both had grainy dispersed parts which could be indicative of molybdenum oxide particles (Fig. 5-4), similar morphology was also observed by Vasilopoulou *et al.* [49]. The dispersion of Mo could be a reason for observing a higher reduction in BET surface area with Mo containing samples (Table 5-1). This grainy texture was absent in both parent SBA-15 (Fig. 5-3) and tungsten containing (Fig. 5-5) samples. However, there was not any clear difference observed in the SEM images of WO_3/SBA-15 and WN/SBA-15 samples (Fig. 5-5).

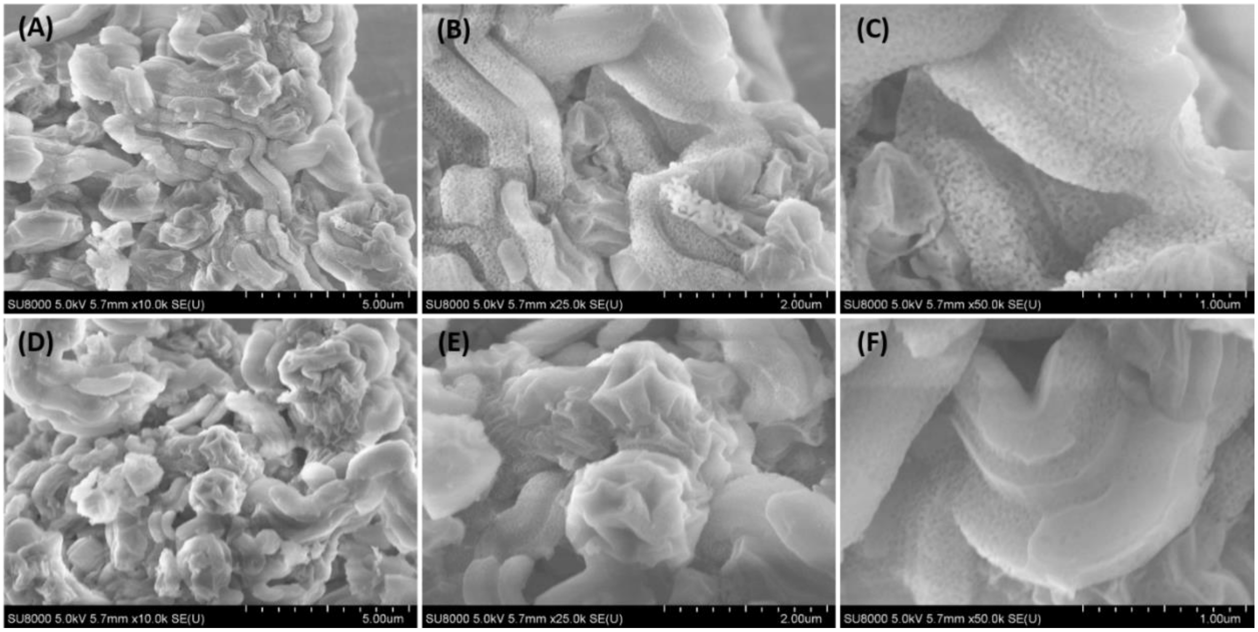

Fig. 5-4: SEM images of fresh (A–C) Mo and (D–F) MoN catalysts.

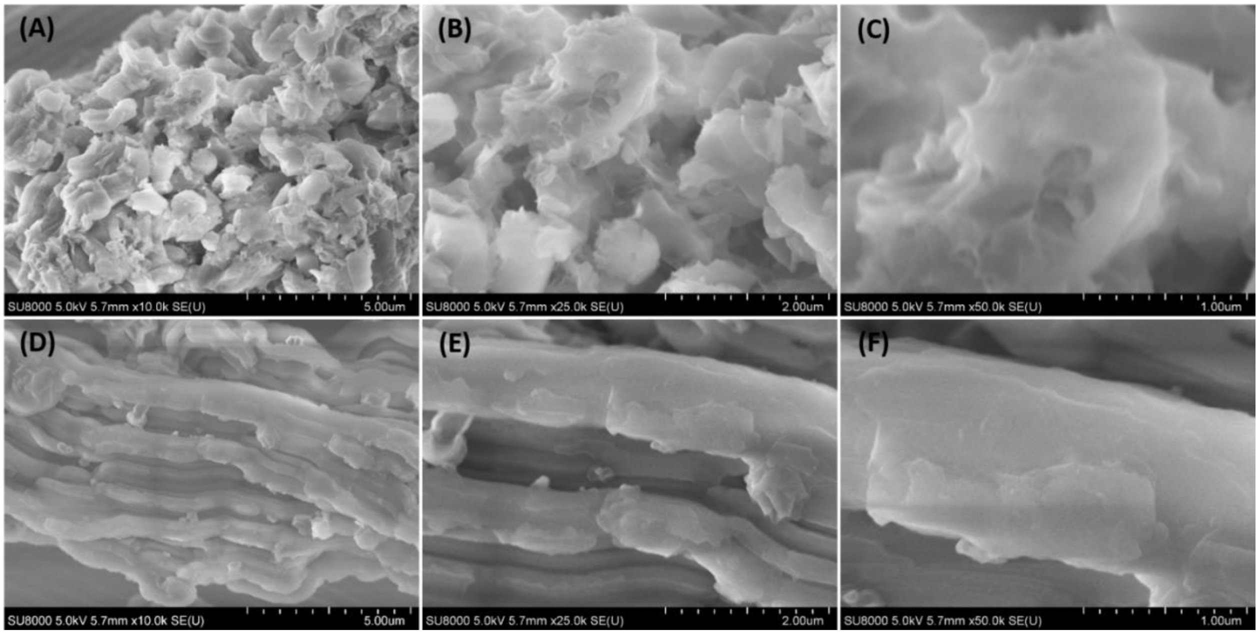

Fig. 5-5: SEM images of fresh (A–C) W and (D–F) WN catalysts

It was difficult to locate tungsten metal in the sample. But using BSE mode, tungsten was observed in spots far apart on the support and structured as a large crystal of tungsten nitride (Fig. 5-6). This confirms the sharp peaks observed with XRD which could be due to the large crystals (section 5.2.2).

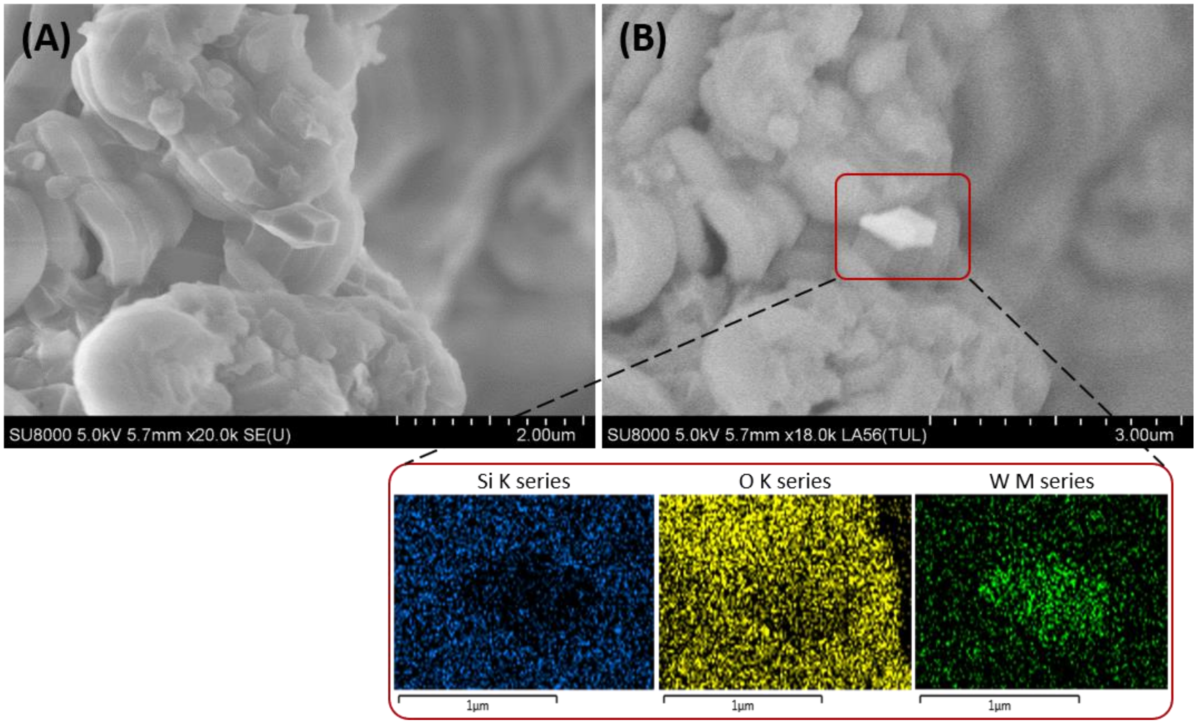

Fig. 5-6: (A) SEM, (B) SEM-BSE, and (C) EDS (inset) analysis for WO3/SBA-15

The existence and composition of the metals present in the samples were analyzed with SEM-EDS. The elemental peaks were shown for molybdenum (Fig. 5-7A and B) and tungsten (Fig. 5-7C and D) metal oxides and nitrides with 4 wt% target loading on SBA-15. SEM-EDS confirmed the existence of both molybdenum and tungsten nitride species. The elemental composition of molybdenum in Mo/SBA-15 closely matched with the initial loading of 4 wt% (Table 5-3). The high tungsten metal content in WO_3/SBA-15 is due to the mapping section chosen which was taken around the area where the large tungsten crystal was observed. The low amount of tungsten in WN/SBA-15 samples could also be due to the mapping area chosen and also that tungsten atoms formed large agglomerates during the synthesis and were observed in spots far away from each other (Fig. 5-6).

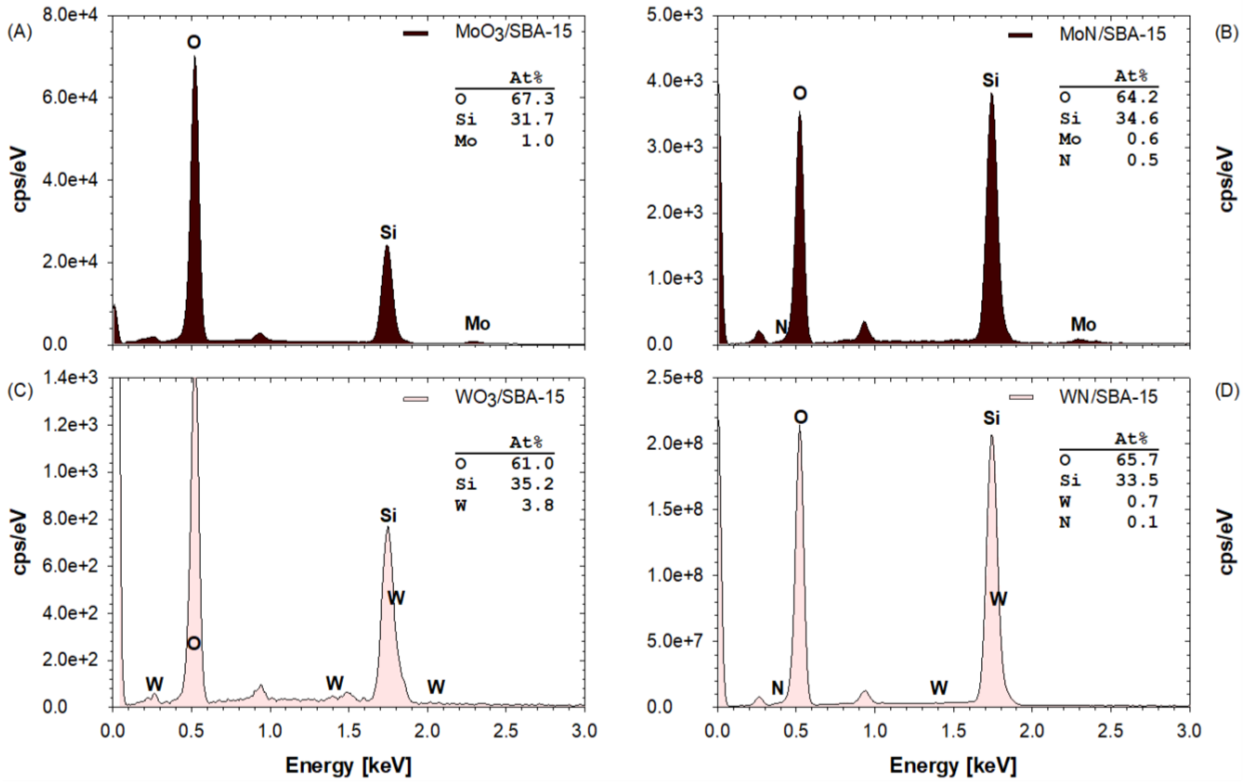

Fig. 5-7: EDS analysis for fresh molybdenum (A) oxide and (B) nitride, and fresh tungsten (C) oxide and (D) nitride catalysts supported on SBA-15 with 4 wt% metal loading.

Table 5-3: Elemental composition of catalysts based on EDS measurements.

Sample	**EDS results [At%]**					surface	target
	Mo	**W**	**O**	**Si**	**N**	**[wt%][a]**	**[wt%][b]**
MoO_3/SBA-15	1.0	-	67.3	31.7	-	3.1	4.0
MoN/SBA-15	0.6	-	64.2	34.6	0.5	1.8	
WO_3/SBA-15	-	3.8	61.0	35.2	-	9.6	4.0
WN/SBA-15	-	0.1	65.7	33.5	0.7	0.3	

[a] based on EDS metal loading wt% (surface)
[b] target metal loading in wt% (bulk)

5.2.4 XPS

A batch of 20 wt% MoO_3/SBA-15 and WO_3/SBA-15 were prepared in order to get peaks with higher resolution and intensity for the XPS analysis. The nitride samples were prepared by reducing with ammonia. XPS was used to determine the chemical state of the metal catalysts and to confirm whether the oxide or nitride form of the Mo and W exists in the catalyst. The binding energies of W 4f and Mo 3d peaks in the XPS spectra can verify the state of molybdenum and tungsten oxides or nitrides (Fig.

5-8). The peaks at around 232 and 236 eV are associated with the molybdenum oxide (Fig. 5-8A), and the peaks at around 36 and 38 eV are related to the tungsten oxide (Fig. 5-8C) [50]. The shift from higher binding energy to a lower binding energy peak in both molybdenum and tungsten samples is indicative of the metal being reduced (Fig. 5-8A) [51]. In the case of molybdenum, the two peaks at around 228 and 231.5 eV, and in the case of tungsten, the peaks at the binding energies of 32.5 and 34 eV confirm the presence of reduced metals in the catalyst. However, a peak at around 236 eV for molybdenum and a broad peak at 36 eV and a weak peak at 38 confirms the presence of a low amount of metal oxide in the reduced samples. Nonetheless, peak deconvolution would not provide accurate quantitative information due to the low intensity of the signals, which is attributed to the low loading of the metals.

On the other hand, the N1s peak in a metal nitride appears at around 397 eV, while nitrogen bonded to Si shows a peak in the range of 398 to 402.5 eV [52]. The nitrogen peak in the WN/SBA-15 catalyst (Fig. 5-8D) confirmed the existence of nitrides with the binding energy of N1s from 396 to 400 eV [52]. However, the nitrogen peak was not prominent in the nitride catalyst of MoN/SBA-15 (Fig. 5-8B), which could be due to the high dispersion of the metal on the support. Plots for the 4 wt% loading samples are presented in Fig. A-5

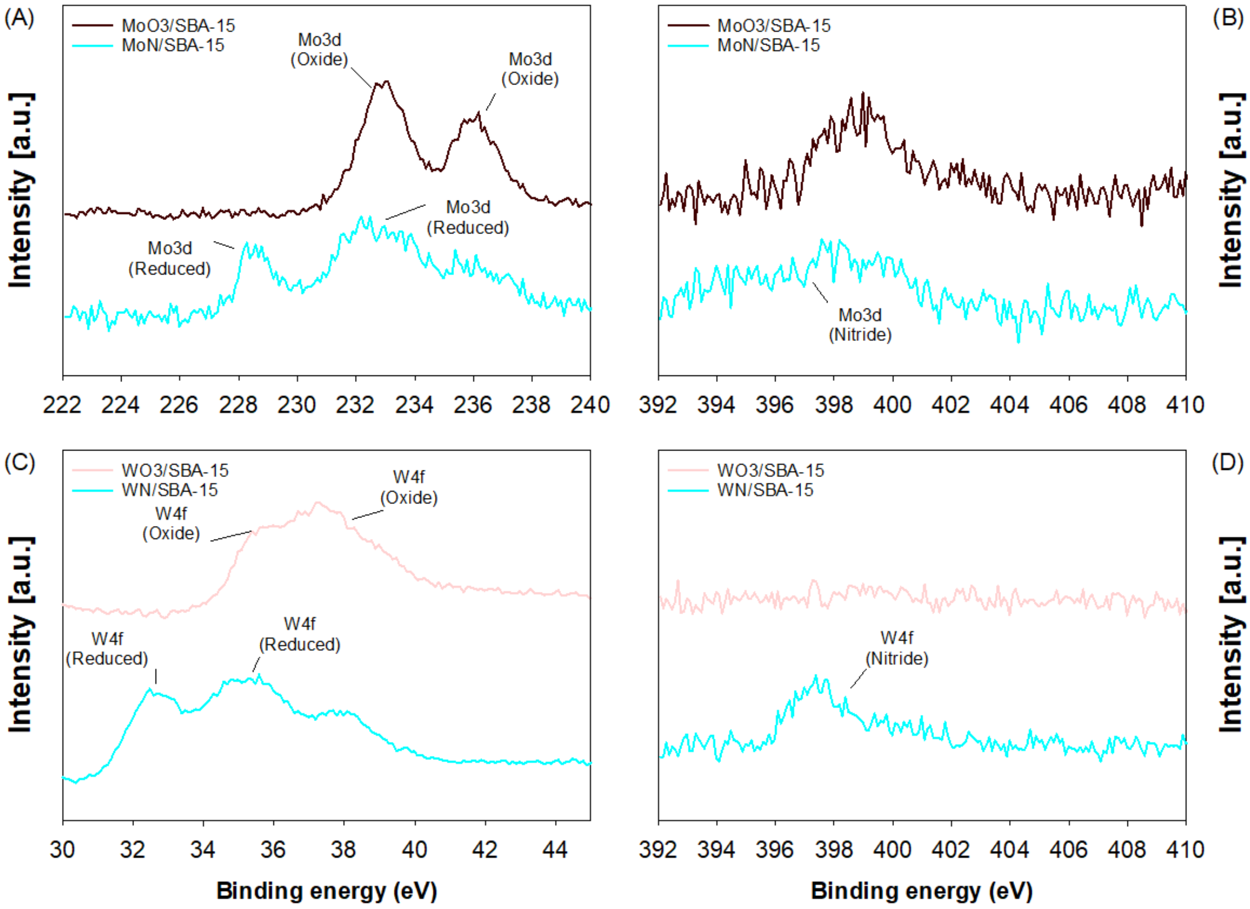

Fig. 5-8: XPS plot of 20 wt% loading for (A) molybdenum oxide and nitride catalysts showing Mo and (B) N spectra. Plot (C) shows tungsten oxide and nitride catalyst peaks corresponding to W and (D) N spectra.

5.2.5 Temperature-programmed oxidation

Temperature-programmed oxidation was performed on the prepared fresh catalysts and the support (SBA-15) to further verify the existence of nitrides. A blank run was performed, and the curve was subtracted from the results to eliminate the effect of an empty crucible. Theoretically, a weight increase of 1.63% and 0.64% is expected when Mo and W nitrides are converted to their corresponding Mo and W oxides. The assumptions are that (1) metal nitrides are only in the form of Mo_2N and W_3N_4 based on the XRD results (see Fig. 5-2, section 5.2.2), (2) all of the metals were converted to their nitrides, (3) prepared nitride samples stayed in nitride form during storage (there was a week gap between preparation and the test), and (4) that MoO_3 and WO_3 are the only corresponding forms of oxides for molybdenum and tungsten samples respectively. To verify that the difference in plots was only due to the changes from the metals, a plot of SBA-15 is also shown, which was exposed to the same environment and temperature as the catalysts, showing the plot being practically flat (Fig. 5-9). GaN catalyst had shown weight increase during regeneration with air due to GaN oxidation, as discussed in section 4.2. As expected, there was a weight increase only in the MoN/SBA-15 and WN/SBA-15 samples which represents the oxidation of the nitrides. There was a difference of approximately 200 °C in temperatures at which the weight changes occurred (280 °C for MoN/SBA-15 and 475 °C for WN/SBA-15), which was also observed with the TPO done on the spent catalysts (5.4.1, Fig. 5-15). This could be due to the type of coke that was formed on the catalyst and the C–N interaction during the formation of coke species.

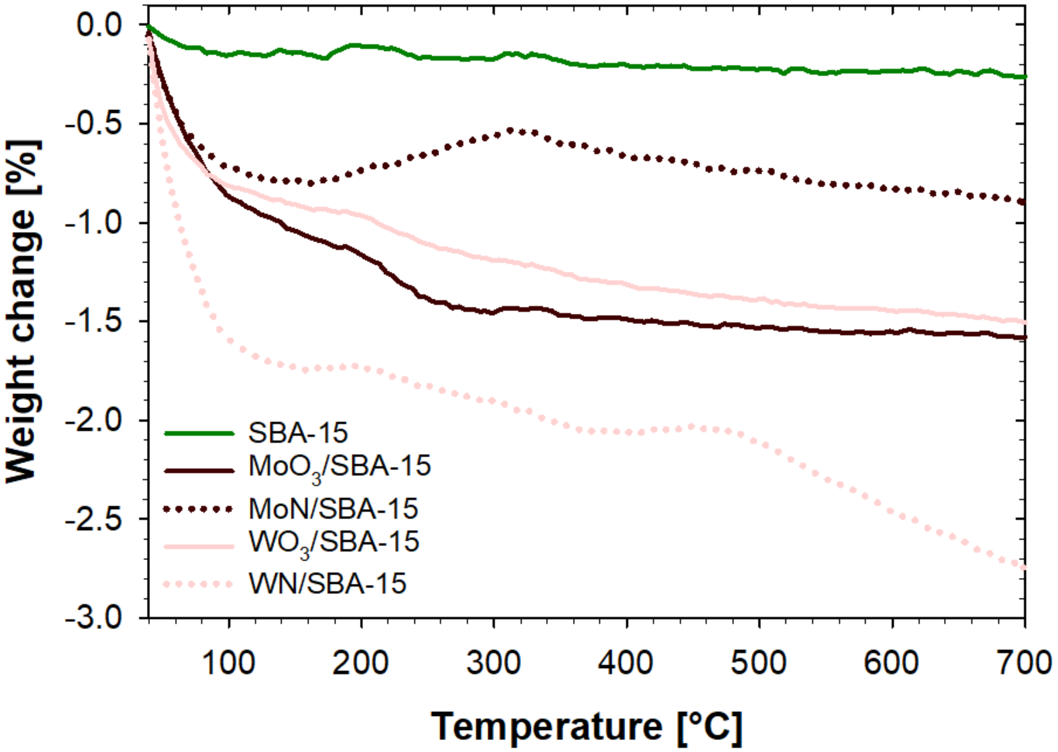

Fig. 5-9: TPO of SBA-15 and fresh oxide and nitride catalysts under air at 1 °C min⁻¹.

5.3 Activity measurements

The reduced molybdenum containing catalyst showed an increase in CH_4 conversion for the initial 2 h on stream reaching up to a maximum value of 1.8% and then decreased asymptotically to steady values of around 0.2–0.6% (Fig. 5-10 A–D). There was no initial increase in CH_4 conversion for the single metal W/SBA-15 catalyst (Fig. 5-10C). This could be due to the formation of molybdenum carbide in the initial stage. However, the nitride catalyst did not exhibit the initial increase in the beginning and started decreasing from the early hours on stream until reaching a steady value around 0.1–0.2% (Fig. 5-10 E–H). For comparison, the supported bimetallic $PtSn/SiO_2$ catalyst in Dumesic's group had a maximum conversion of 0.1% (typically less) after 6 h TOS at 700 ºC with only CH_4 as feed and 6 wt% Pt loading (Pt:Sn atomic ratio of 3:1) [21]. Also, methane conversion on GaN/SBA-15 700 ºC in Dutta's work reached a steady-state conversion of 0.18% after 7 h TOS with catalyst loading of 16 wt% and 80% CH_4 used as feed [31].

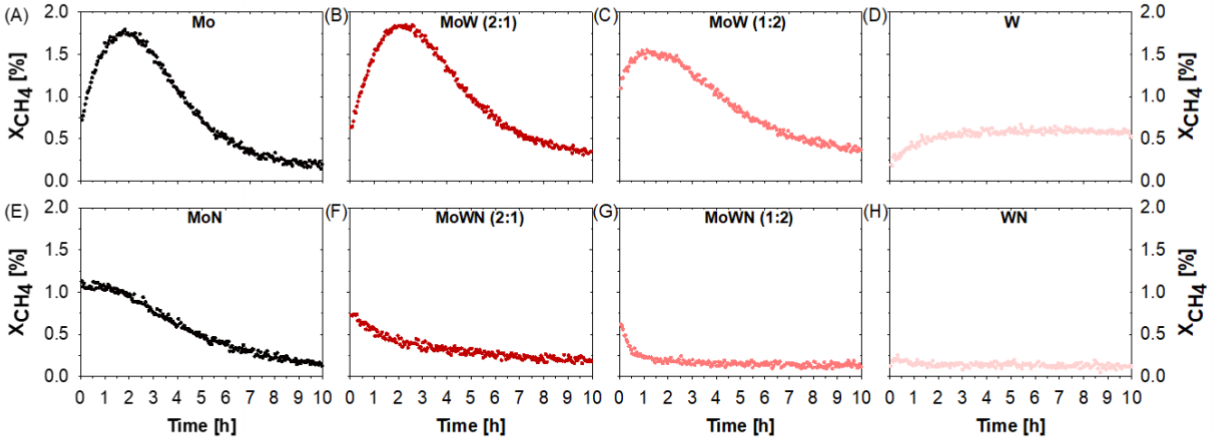

Fig. 5-10: Conversion as a function of time on stream [h] for (A–D) metal and (E–H) metal nitride catalysts activated with 50 vol% CH4 (total = 8 ml min^{-1}) at 700 ºC.

Catalysts that contained molybdenum mainly favored benzene formation with the highest rate of approximately 90% observed at the start of the experiment and gradually reduced to approximately 60% while ethylene selectivity increased to about 40%. However, after the first hour, the W/SBA-15 had a fairly stable selectivity of 60% and 30% for benzene and tungsten respectively (Fig. 5-11D).

Propylene, toluene, and naphthalene selectivity were constant for all the metal/mixed-metal catalysts and much lower than benzene and ethylene (Fig. 5-11 A–D). Nitride catalyst had a more stable trend with MoN/SBA-15 (Fig. 5-11E) showing no selectivity towards benzene and WN/SBA-15 (Fig. 5-11H) initially had high ethylene selectivity which decreased with time on stream. Increasing tungsten content increased the selectivity for ethylene and propylene.

For 10 h activation time, starting from Mo/SBA-15, the average conversion to hydrocarbons increased and with the addition of tungsten. The maximum conversion to hydrocarbon was observed with MoW(1:5)/SBA-5 (Fig. 5-12A) which also had the highest TOF (see Table 5-4). This suggests that there is a synergistic effect when Mo and W metals are mixed as a catalyst. The nitride catalyst showed a trend where the activity decreased with increasing tungsten content (Fig. 5-12B). The nitride catalysts showed lower activity towards methane conversion with the highest value of 0.55% for MoN/SBA-15 and WN/SBA-15 having the lowest value of 0.14% (Fig. 5-12B). The nitride catalyst showed a declining trend with decreasing Mo content.

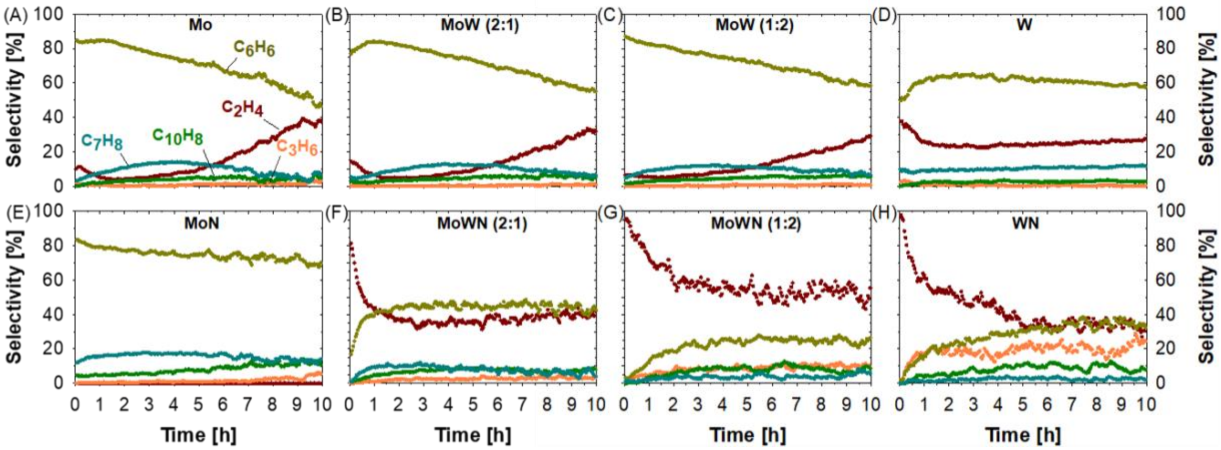

Fig. 5-11: Selectivity as a function of time on stream [h] for (A–D) metal and (E–H) metal nitride catalysts activated with 50 vol% CH_4 (total = 8 ml min^{-1}) at 700 °C.

TGA was used to measure the total coke content for the 10 h on stream with MoW(2:1)/SBA-15 having the highest coke content (189.2 $mg_{Coke}\ g_{Cat}^{-1}$) and W/SBA-15 having the least amount of coke deposition (111.1 $mg_{Coke}\ g_{Cat}^{-1}$) on the catalyst (Fig. 5-12A). The coke content for the nitride catalysts showed a decreasing trend with increasing W content, with WN/SBA-15 exhibiting the lowest amount of total coke (8.2 $mg_{Coke}\ g_{Cat}^{-1}$) at the end of 1 h TOS. Both coke and activity decreased with the addition of tungsten, but the ratio of total coke per HC conversion increased and was higher for the nitride catalysts compared to the metal catalysts (Table 5-4). The 10 h (MoWN(4:1)/SBA-15 has 13 h activation) average values for the activity, selectivity, coke content, and TOF for all the measured samples are summarized in Table 5-4. In comparison with the catalysts from Dumesic's group, our nitride catalyst for 10 h TOS had coke content in the range of 8–70 $mg_{Coke}\ g_{Cat}^{-1}$ for WN/SBA-15 and MoN/SBA-15 respectively, while for a slightly less time of 6 h activation, Dumesic's group reported 66–87 $mg_{Coke}\ g_{Cat}^{-1}$ for their PtSn/SiO_2 and Pt/SiO_2 catalysts respectively [21]. The supported GaN/SBA-15 showed 6 $mg_{Coke}\ g_{Cat}^{-1}$ for a 7 h TOS at 700 °C [37].

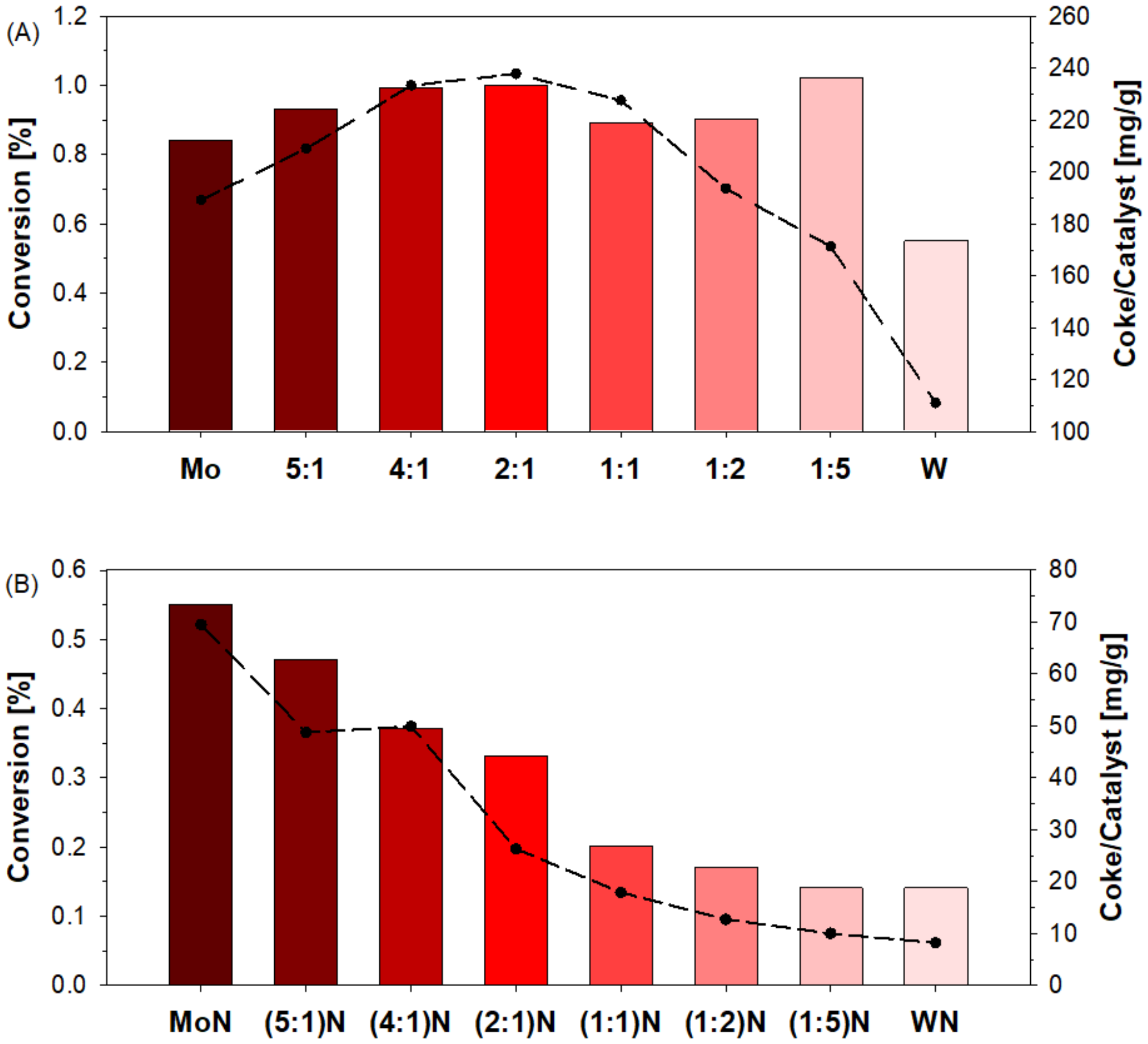

Fig. 5-12: Average conversion to HC and total coke content for 10 h activation on spent (A) metal and (B) metal nitride catalysts. Note (4:1)N was activated for 13 h. Dashed line for guidance only.

The average 10 h values for the metal and mixed-metal catalysts were similar results in terms of selectivity and mainly favored benzene production. The only difference was observed with the W/SBA-15 catalyst which showed a higher selectivity towards ethylene (Fig. 5-13A).

Nevertheless, the nitride catalysts showed an increasing selectivity towards ethylene when moving towards more tungsten content, but the maximum ethylene production was observed with slight mixing of Mo metal in the MoWN(1:5)/SBA-15 catalyst shifting ethylene from 42 to 65% indicating a synergistic effect of mixing metals (Fig. 5-13B). The observed trend for nitride catalysts was that the average selectivity favored mainly heavier hydrocarbon products (benzene and naphthalene) with increasing Mo content while increasing W ratio favored mainly lighter hydrocarbons (ethylene and propylene) (Fig. 5-13B). The decrease in ethylene formation for the WN sample compared to the MoWN (1:5) might be due to the larger WN-crystallite size, which can result in a lower specific surface area of the WN catalyst. But at this point, the hypothesize cannot be confirmed.

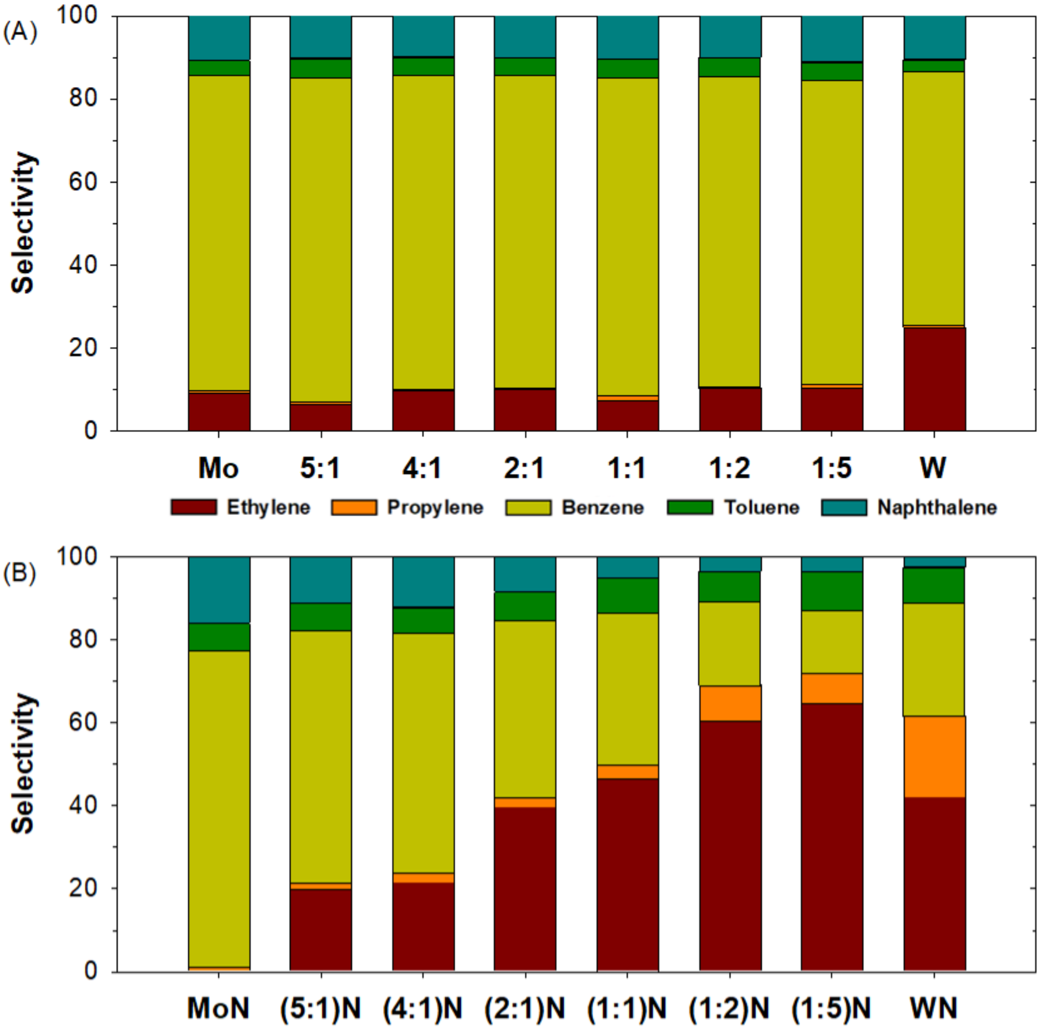

Fig. 5-13: Average selectivity of 10 h activation for (A) metal and (B) metal nitride catalysts.

Table 5-4: Overall and hydrocarbon (HC) selectivity, methane conversion, molar species out, total coke and turn over frequency (TOF) for supported catalysts.

Catalyst		**Overall selectivity [%]**					**X_{CH4}-HC [%]**	**X_{CH4}-Coke [%]**	**TOF [h^{-1}]**	**Total Coke[a] [$mg_{Coke}\ g_{Cat}^{-1}$]**
		C_2H_4	**C_3H_6**	**C_6H_6**	**C_7H_8**	**$C_{10}H_8$**	**CH_4**	**CH_4**		
Metals										
Mo		9.22	0.61	75.88	3.53	10.75	0.84	3.36	1.07	189.2
MoW	5:1	6.40	0.66	77.99	4.57	10.38	0.93	4.01	1.34	209.0
	4:1	9.63	0.34	75.81	4.26	9.96	0.99	4.06	1.49	233.4
	2:1	9.89	0.30	75.47	4.15	10.18	1.00	4.17	1.65	237.9
	1:1	7.38	1.22	76.58	4.35	10.46	0.89	3.59	1.66	227.6
	1:2	10.27	0.38	74.78	4.37	10.19	0.90	3.06	1.84	193.7
	1:5	10.27	0.88	73.30	4.31	11.25	1.02	2.88	2.26	171.4
W		24.93	0.51	61.30	2.72	10.54	0.55	1.94	1.28	111.1
Metal-nitrides										
MoN		0.00	1.07	76.08	6.68	16.16	0.55	1.22	0.68	69.5
MoWN	5:1	19.65	1.46	61.10	6.41	11.38	0.47	0.93	0.67	48.7
	4:1	21.44	2.32	57.90	6.17	12.17	0.37	0.68	0.54	49.9
	2:1	39.65	2.43	42.59	6.91	8.43	0.33	0.58	0.53	26.3
	1:1	46.35	3.38	36.57	8.38	5.31	0.20	0.46	0.34	17.9
	1:2	60.37	8.58	20.28	7.09	3.68	0.17	0.28	0.35	12.7
	1:5	64.53	7.52	15.17	9.05	3.73	0.14	0.23	0.30	10.0
WN		42.04	19.50	27.50	8.37	2.59	0.14	0.22	0.32	8.2

5.4 Characterization of spent catalyst

5.4.1 Temperature-programmed oxidation

Temperature-programmed oxidation coupled with mass spectroscopy (TPO-MS) was used to qualitatively validate the combustion process for the spent catalysts. Fig. 5-14 shows the TPO results of the spent MoN/SBA-15 showing the mass change from TGA, and CO_2 and H_2O signals from the MS. Only CO_2 and H_2O signals were observed at the point where the mass decreased due to coke combustion, as a result, for further TPO test no MS was used, and this enabled us to free resources and use the lab instruments in an efficient manner.

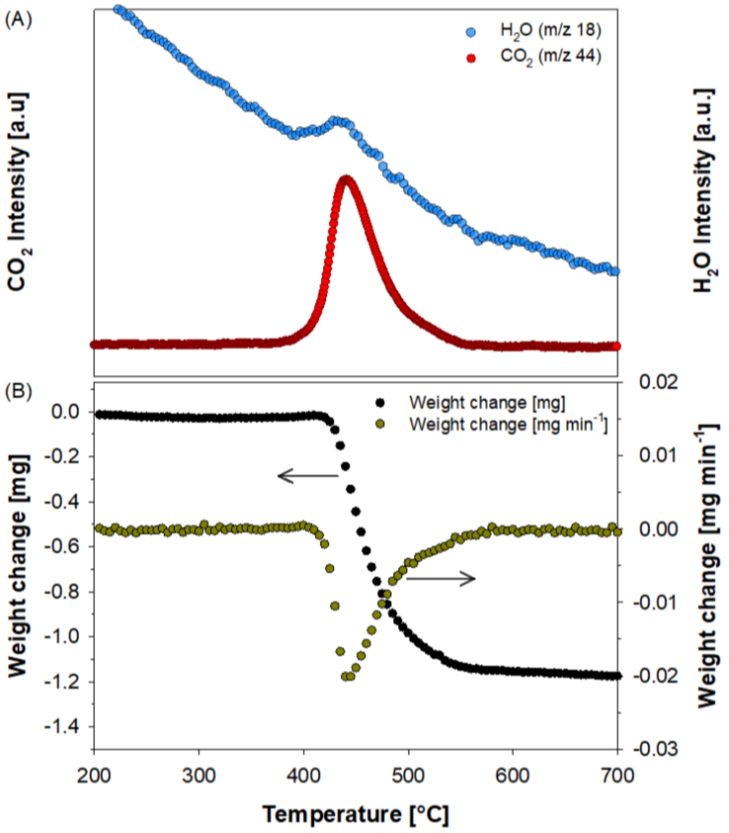

Fig. 5-14: (A) MS signals for H_2O (m/z 18) and CO_2 (m/z 44) and (B) TGA weight change for spent MoN/SBA-15.

The differential thermogravimetry (DTG) curves for the spent metal and mixed-metal oxides and nitride catalysts burning coke are represented in Fig. 5-15. There is a distinct temperature difference of around 100 °C between the peaks from Mo/SBA-15 and W/SBA-15 samples. This is evidence that there are two types of carbonaceous species existing as coke. The low temperature peak in molybdenum is associated with the carbonaceous MoC_x species [53], [54]. The single metal catalysts showed less of the double peak indicating less more of single type carbonaceous species formed. Furthermore, it is also suggested that the low temperature peak is due MoC_x species that is used for C–H activation while the high temperature peaks are responsible for the deactivation [55].

The same trend as in the oxide catalyst was shown with the metal-nitride catalysts with much lower intensity (Fig. 5-15B). The lower intensity shows the lower amount of coke was burnt from the catalyst (Table 5-4). In the case of W/SBA-15, the peak in Fig. 5-15 was very low but when the same catalyst was used for 40 h, the peak appeared in the same spot but much more distinct. The temperature range at which the coke was burnt indicated that the deposited coke were amorphous and not graphitic [56].

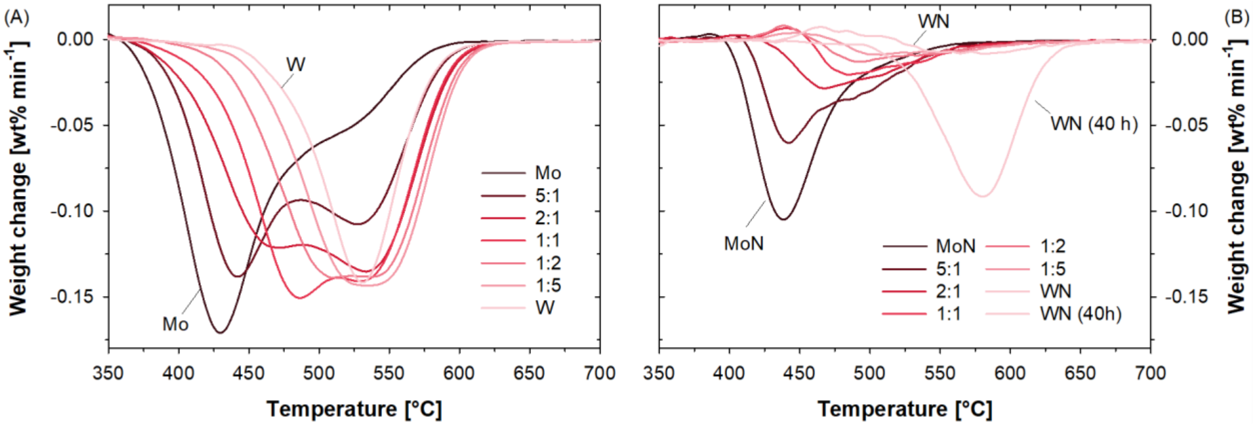

Fig. 5-15: DTG curves for the temperature-programmed oxidation of spent (A) metal and (B) metal-nitride catalysts supported on SBA-15.

Chapter 6

6 Conclusion and future work

6.1 GaN catalyst

The regeneration capability of the supported and unsupported gallium nitride catalysts was assessed. The results showed the catalyst could be successfully regenerated and reused with air while maintaining ethylene yield. This included regeneration with air as an oxidative medium to burn off the coke and replenishment with re-nitridation cycles. Air was compatible due to the low temperature required for regeneration without bulk oxidation of the catalyst. There was an oxide layer of Ga_2O_3 formed on the surface after regeneration which resulted in unwanted H_2O and CO_x species in the outlet. This was prevented by once again nitridation of the catalyst post regeneration.

6.2 MoW and MoWN catalysts

Molybdenum and tungsten metals were investigated for their catalytic activation towards methane conversion. Catalyst screening was done with Mo and W single metal and mixed-metal catalyst with Mo:W ratios ranging from 5:1 to 1:5 impregnated on SBA-15 support. Also, another set of samples was prepared that were pretreated with ammonia gas to form their corresponding nitride catalysts. In this work two main issues in catalyst performance were addressed, selectivity and coke deposition The catalysts were evaluated by means of characterization tests and activity tests with methane at 700 °C.

The nitride peaks showing successful nitridation were confirmed using SEM, EDS, XRD, and XPS. The SEM results showed molybdenum stayed dispersed, while tungsten metal on SBA-15 agglomerated to large crystals (strong peaks in XRD). For a 10 h time on stream, the oxide catalysts showed a maximum conversion of 1.02% with mostly favoring benzene production, the lesser being ethylene, propylene, toluene, and naphthalene. The nitride catalyst reduced the coke to up to 8 mg_{Coke}/g_{Cat} (for WN/SBA-15 sample) and the selectivity was increased from 25% ethylene with metal/mixed-metal catalyst to 65% ethylene with the nitride catalysts. The highest selectivity was achieved with the MoW (5:1)/SBA-15 suggesting synergistic effects when both metals were co-impregnated. In general, the more Mo content produced more of the heavier hydrocarbons (benzene, naphthalene), while increasing the tungsten content favored more of the lighter products (ethylene and propylene). As a result, promising results were achieved with Mo and W loaded catalysts rather than going for the more expensive rare precious metal catalysts such as Pt or Ga.

6.3 Future work

The work proved that we could tailor catalysts to our needs by changing the metal ratios. However, there is still room for optimization in different stages of the process from synthesis to activity test.

For instance, it is hypothesized that the pore size can affect selectivity and affect oligomerization of products in methane activation. SBA-15 is versatile and can be synthesized with changing parameters such as gel composition and temperature that would lead to different morphology and pore size that could affect selectivity towards methane activation. Preliminary testing showed that Mo or W metals supported on ZSM-5 had higher activity compared to SBA-15 products mainly favored benzene. We could exploit the activity of zeolite and tailor the catalyst for a desired product through pretreatments such as nitridation may be investigated.

In the case of catalyst synthesis, impregnation of bimetallic catalyst can either be done together or as two separate impregnations followed by calcination steps for each metal. The applies to the drying and calcination steps, a physical crushing and mixing of the catalyst can assist for better dispersion of the metal when calcining.

The optimum nitridation temperature was found for gallium catalyst and they were different depending on whether the catalyst was supported or unsupported. This could mean that the same could apply to the Mo and W catalysts that could be further investigated for best results. Also, it was observed that Mo containing catalysts were very effective in breaking ammonia during nitridation and the effect decreased with increasing W content (Fig. A-10).

Nomenclature

Latin symbols

$c_{s,i}$	mol m^{-3}	concentration of the ith species on the surface
C_{ads}	mg g_{cat}^{-1}	adsorbed carbonaceous surface intermediates
d_{pore}	µm	particle diameter
d_{pore}	nm	pore diameter
E_A	kJ mol^{-1}	activation energy
ΔG_R^o	kJ mol^{-1}	standard free energy of reaction at 298.15 K
GHSV	differ	gas hourly space velocity
h_{Bed}	cm	catalyst bed height
ΔH_R^o	kJ mol^{-1}	standard heat of reaction at 298.15 K
ID	cm	inner diameter of the quartz reactor
m_{cat}	g	mass of catalyst loaded
M_i	g mol^{-1}	molar mass of the ith component
MFC	−	mass flow controller (for gases)
n	−	order of the reaction
n_i^0	mol	number of moles of the ith component at time $t = 0$
$\dot{n}_{i,in}$	mol min^{-1}	inlet molar flow rate of the ith component
$\dot{n}_{i,out}$	mol min^{-1}	outlet molar flow rate of the ith component
n_N	mol	number of moles of nitrogen in the nitride catalyst
p_i	bar	partial pressure of the ith gas species
r	mol min^{-1} g_{cat}^{-1}	rate of reaction
r_{obs}	mol min^{-1} g_{cat}^{-1}	observed rate of reaction
$\mathcal{R}$	J K^{-1} mol^{-1}	universal gas constant = 8.314
S_i	−	selectivity of the ith species
T	K	temperature

V_{cat}	ml	volume of the catalyst bed
$\dot{V}_{i,in}$	$ml_N\ min^{-1}$	volumetric flow rate of the i^{th} gas species at normal conditions
$WHSV$	differ	weight hourly space velocity
X_{CH_4}	–	methane conversion
Y_i	–	product yield

Greek symbols

ε	–	bed porosity
η	–	approach to equilibrium
η_{eff}	–	effectiveness factor
Ψ_i	–	weisz modulus for the i^{th} component
φ_P	–	sphericity
Φ	–	Thiele modulus
ν_i	–	number of carbon atoms in the i^{th} hydrocarbon species
ρ_{Bulk}	$g\ ml^{-1}$	bulk density of the catalyst
τ	–	tortuosity

Other

*	–	empty active site
CH_3*		occupied site (e.g., methyl group)

Subscripts and superscripts

ads	adsorbed
Bed	catalyst bed
$Bulk$	catalyst bulk property
c	carbon
cat	catalyst
eqm	equilibrium
N	normal conditions, 273.15 K and 1.013 bar
tot	total

Abbreviation

BSE	backscattered electron
CP	cross-polarization
DFT	density functional theory
DHA	dehydroaromatization
DRIFTS	diffuse reflectance infrared Fourier transform spectroscopy
DTG	differential thermogravimetric
EDS	energy-dispersive X-ray spectroscopy

EISA	evaporation induced self-assembly
FBR	fixed bed reactor
FID	flame ionization detector
FTIR	Fourier transform infrared
GHSV	gas hourly space velocity
HRTEM	high-resolution transmission electron microscopy
ICDD	International Centre for Diffraction Data
ICP	inductively coupled plasma
IR	infrared
MAS	magic angle spinning (in NMR)
MS	mass spectrometry
OCM	oxidative coupling of methane
PDF	powder diffraction file
SEM	scanning electron microscopy
SEM	secondary electron multiplier (in MS)
SS-NMR	solid-state nuclear magnetic resonance
STEM	scanning transmission electron microscopy
TCD	thermal conductivity detector
TEM	transmission electron microscopy
TEOS	tetraethyl orthosilicate
TGA	thermogravimetric analysis
TI	temperature indicator
TIC	temperature indicator controller
TPD	temperature-programmed desorption
TP-DRIFTS	temperature-programmed DRIFTS
TPO	temperature-programmed oxidation
TPR	temperature-programmed reduction
TPSR	temperature-programmed surface reaction
XPS	x-ray photoelectron spectroscopy
XRD	X-ray diffraction

Gas species (mass-to-charge ratio, m/z)

	Name	**m/z**
H_2	hydrogen	2
HD	hydrogen isotope	3
D_2	hydrogen isotope (deuterium)	4
CO	carbon monoxide	28
CO_2	carbon dioxide	44
CH_4	methane	15, 16
$^{13}CH_4$	carbon labeled methane	16, 17
CH_3D	methane isotope	16, 17

CD_4	methane isotope	18, 20
C_2H_4	ethylene	28
C_2D_4	ethylene isotope	32
C_2H_6	ethane	30
C_2D_6	ethane isotope	36
C_3H_6	propylene	42
C_6H_6	benzene	78
C_6D_6	benzene isotope	84
C_7H_8	toluene	91
$C_{10}H_8$	naphthalene	120
H_2O	water	18
N_2	nitrogen	28
NH_3	ammonia	17
Ar	argon	40, 20

References

[1] J. Baltrusaitis, I. Jansen, J.D. Schuttlefield Christus, Renewable energy based catalytic CH4 conversion to fuels, Catal. Sci. Technol. 4 (2014) 2397. https://doi.org/10.1039/c4cy00294f.

[2] U.S. Energy Information Administration (EIA), (n.d.). https://www.eia.gov/tools/faqs/faq.php?id=52&t=8 (accessed July 5, 2021).

[3] Natural Gas Facts, Natural Resources Canada, (n.d.). https://www.nrcan.gc.ca/science-data/data-analysis/energy-data-analysis/energy-facts/natural-gas-facts/20067 (accessed August 1, 2021).

[4] B.J. Michaud, ENERGY IN QUEBEC WHAT ROLE FOR NATURAL GAS IN THE CONTEXT OF ELECTRIFICATION ?, 2020. https://www.iedm.org/energy-in-quebec-what-role-for-natural-gas-in-the-context-of-electrification/.

[5] K. Velebná, M. Horňáček, V. Jorík, P. Hudec, M. Čaplovičová, L. Čaplovič, The influence of molybdenum loading on activity of ZSM-5 zeolite in dehydroaromatization of methane, Microporous Mesoporous Mater. 212 (2015) 146–155. https://doi.org/10.1016/j.micromeso.2015.04.001.

[6] K. Mascarenhas, Examining the expansion potential of the petrochemical industry in canada, 2015. https://ceri.ca/assets/files/Study_153_Full_Report.pdf (accessed July 21, 2019).

[7] S. McGrath, IBISWorld Industry Report 32521CA Plastic & Resin Manufacturing in Canada, (2019). https://www.ibisworld.com (accessed July 14, 2021).

[8] N. Leach, IBIS World Industry Report 32511CA Petrochemical Manufacturing in Canada, (2019). https://www.ibisworld.com (accessed July 14, 2021).

[9] Z.R. Ismagilov, E. V. Matus, M.A. Kerzhentsev, L.T. Tsikoza, I.Z. Ismagilov, K.D. Dosumov, A.G. Mustafin, Methane conversion to valuable chemicals over nanostructured Mo/ZSM-5 catalysts, Pet. Chem. 51 (2011) 174–186. https://doi.org/10.1134/s0965544111020058.

[10] S. Ma, X. Guo, L. Zhao, S. Scott, X. Bao, Recent progress in methane dehydroaromatization: From laboratory curiosities to promising technology, J. Energy Chem. 22 (2013) 1–20. https://doi.org/10.1016/S2095-4956(13)60001-7.

[11] B.L. Farrell, V.O. Igenegbai, S. Linic, A Viewpoint on Direct Methane Conversion to Ethane and Ethylene Using Oxidative Coupling on Solid Catalysts, ACS Catal. 6 (2016) 4340–4346. https://doi.org/10.1021/acscatal.6b01087.

[12] P. Schwach, X. Pan, X. Bao, Direct Conversion of Methane to Value-Added Chemicals over Heterogeneous Catalysts: Challenges and Prospects, Chem. Rev. 117 (2017) 8497–8520. https://doi.org/10.1021/acs.chemrev.6b00715.

[13] C. Karakaya, R.J. Kee, Progress in the direct catalytic conversion of methane to fuels and chemicals, Prog. Energy Combust. Sci. 55 (2016) 60–97. https://doi.org/10.1016/j.pecs.2016.04.003.

[14] P. Tang, Q. Zhu, Z. Wu, D. Ma, Methane activation: the past and future, Energy Environ. Sci. 7 (2014) 2580. https://doi.org/10.1039/C4EE00604F.

[15] X. Guo, G. Fang, G. Li, H. Ma, H. Fan, L. Yu, C. Ma, X. Wu, D. Deng, M. Wei, D. Tan, R. Si, S. Zhang, J. Li, L. Sun, Z. Tang, X. Pan, X. Bao, Direct, nonoxidative conversion of methane to ethylene, aromatics, and hydrogen., Science. 344 (2014) 616–9. https://doi.org/10.1126/science.1253150.

[16] N. Kosinov, F.J.A.G. Coumans, G. Li, E. Uslamin, B. Mezari, A.S.G. Wijpkema, E.A. Pidko, E.J.M. Hensen, Stable Mo/HZSM-5 methane dehydroaromatization catalysts optimized for high-temperature calcination-regeneration, J. Catal. 346 (2017) 125–133. https://doi.org/10.1016/J.JCAT.2016.12.006.

[17] H. Sheng, E.P. Schreiner, W. Zheng, R.F. Lobo, Non-oxidative Coupling of Methane to Ethylene Using Mo2C/[B]ZSM-5, ChemPhysChem. 19 (2018) 504–511. https://doi.org/10.1002/cphc.201701001.

[18] J.J. Spivey, G. Hutchings, Catalytic aromatization of methane, Chem. Soc. Rev. 43 (2014) 792–803. https://doi.org/10.1039/C3CS60259A.

[19] K. Sun, D.M. Ginosar, T. He, Y. Zhang, M. Fan, R. Chen, Progress in Nonoxidative Dehydroaromatization of Methane in the Last 6 Years, Ind. Eng. Chem. Res. 57 (2018) 1768–1789. https://doi.org/10.1021/acs.iecr.7b04707.

[20] I. Vollmer, B. van der Linden, S. Ould-Chikh, A. Aguilar-Tapia, I. Yarulina, E. Abou-Hamad, Y.G. Sneider, A.I. Olivos Suarez, J.-L. Hazemann, F. Kapteijn, J. Gascon, On the dynamic nature of Mo sites for methane dehydroaromatization, Chem. Sci. 9 (2018) 4801–4807. https://doi.org/10.1039/C8SC01263F.

[21] D. Gerceker, A.H. Motagamwala, K.R. Rivera-Dones, J.B. Miller, G.W. Huber, M. Mavrikakis, J.A. Dumesic, Methane Conversion to Ethylene and Aromatics on PtSn Catalysts, ACS Catal. 7 (2017) 2088–2100. https://doi.org/10.1021/acscatal.6b02724.

[22] Y. Xiao, A. Varma, Highly Selective Nonoxidative Coupling of Methane over Pt-Bi Bimetallic Catalysts, ACS Catal. 8 (2018) 2735–2740. https://doi.org/10.1021/acscatal.8b00156.

[23] A. Sridhar, M. Rahman, S.J. Khatib, Enhancement of Molybdenum/ZSM-5 Catalysts in Methane Aromatization by the Addition of Iron Promoters and by Reduction/Carburization Pretreatment, ChemCatChem. 10 (2018) 2571–2583. https://doi.org/10.1002/cctc.201800002.

[24] J.S.J. Hargreaves, D. Mckay, Catalysis with Nitrides and Oxynitrides, ChemInform. 37 (2006) 84–108. https://doi.org/10.1002/chin.200645265.

[25] J.S.J. Hargreaves, Heterogeneous catalysis with metal nitrides, Coord. Chem. Rev. 257 (2013) 2015–2031. https://doi.org/10.1016/j.ccr.2012.10.005.

[26] Z.-G. Zhang, Process, reactor and catalyst design: Towards application of direct conversion of methane to aromatics under nonoxidative conditions, Carbon Resour. Convers. 2 (2019) 157–174. https://doi.org/10.1016/j.crcon.2019.07.001.

[27] K. Huang, C.T. Maravelias, Synthesis and Analysis of Nonoxidative Methane Aromatization Strategies, Energy Technol. (2019) 1900650. https://doi.org/10.1002/ente.201900650.

[28] A. Galadima, O. Muraza, Advances in Catalyst Design for the Conversion of Methane to Aromatics: A Critical Review, Catal. Surv. from Asia. 23 (2019) 149–170. https://doi.org/10.1007/s10563-018-9262-5.

[29] Y. Chen, X. Mu, X. Luo, K. Shi, G. Yang, T. Wu, Catalytic Conversion of Methane at Low Temperatures: A Critical Review, Energy Technol. (2019) 1900750. https://doi.org/10.1002/ente.201900750.

[30] E.D. Glendening, R. Faust, A. Streitwieser, K.P.C. Vollhardt, F. Weinhold, The Role of Delocalization in Benzene, J. Am. Chem. Soc. 115 (1993) 10952–10957. https://doi.org/10.1021/ja00076a061.

[31] K. Dutta, Structure-activity relationship of gallium nitride for the direct non-oxidative methane coupling to ethylene (PhD thesis, McGill University), (2020) 206.

[32] S. Pimputkar, Gallium nitride, in: Single Cryst. Electron. Mater., Elsevier, 2019: pp. 351–399. https://doi.org/10.1016/b978-0-08-102096-8.00011-2.

[33] Y. Lu, D. Ma, Z. Xu, Z. Tian, X. Bao, L. Lin, A high coking-resistance catalyst for methane aromatization., Chem. Commun. (Camb). (2001) 2048–9. https://doi.org/10.1039/b105853n.

[34] D. Bajec, A. Kostyniuk, A. Pohar, B. Likozar, Nonoxidative methane activation, coupling, and conversion to ethane, ethylene, and hydrogen over Fe/HZSM-5, Mo/HZSM-5, and Fe–Mo/HZSM-5 catalysts in packed bed reactor, Int. J. Energy Res. 43 (2019) 6852–6868. https://doi.org/10.1002/er.4697.

[35] B.J. Lee, Y.G. Hur, D.H. Kim, S.H. Lee, K.-Y.Y. Lee, Non-oxidative aromatization and ethylene formation over Ga/HZSM-5 catalysts using a mixed feed of methane and ethane, Fuel. 253 (2019) 449–459. https://doi.org/10.1016/j.fuel.2019.05.014.

[36] A.L. Dipu, S. Ohbuchi, Y. Nishikawa, S. Iguchi, H. Ogihara, I. Yamanaka, Direct nonoxidative conversion of methane to higher hydrocarbons over silica-supported nickel phosphide catalyst, ACS Catal. 10 (2020) 375–379. https://doi.org/10.1021/acscatal.9b03955.

[37] K. Dutta, V. Chaudhari, C.-J. Li, J. Kopyscinski, Methane conversion to ethylene over GaN catalysts. Effect of catalyst nitridation, Appl. Catal. A Gen. 595 (2020) 117430. https://doi.org/10.1016/j.apcata.2020.117430.

[38] K.S. Wong, J.W. Thybaut, E. Tangstad, M.W. Stoecker, G.B. Marin, Methane aromatisation based upon elementary steps: Kinetic and catalyst descriptors, Microporous Mesoporous

Mater. 164 (2012) 302–312. https://doi.org/10.1016/j.micromeso.2012.07.002.

[39] C. Karakaya, H. Zhu, R.J. Kee, Kinetic modeling of methane dehydroaromatization chemistry on Mo/Zeolite catalysts in packed-bed reactors, Chem. Eng. Sci. 123 (2015) 474–486. https://doi.org/10.1016/j.ces.2014.11.039.

[40] M. V. Luzgin, A.A. Gabrienko, V.A. Rogov, A. V. Toktarev, V.N. Parmon, A.G. Stepanov, The “Alkyl” and “Carbenium” Pathways of Methane Activation on Ga-Modified Zeolite BEA: 13 C Solid-State NMR and GC-MS Study of Methane Aromatization in the Presence of Higher Alkane, J. Phys. Chem. C. 114 (2010) 21555–21561. https://doi.org/10.1021/jp1078899.

[41] L. Li, X. Mu, W. Liu, X. Kong, S. Fan, Z. Mi, C.-J. Li, Thermal non-oxidative aromatization of light alkanes catalyzed by gallium nitride., Angew. Chem. Int. Ed. Engl. 53 (2014) 14106–9. https://doi.org/10.1002/anie.201408754.

[42] V. Chaudhari, K. Dutta, C.-J. Li, J. Kopyscinski, Mechanistic insights of methane conversion to ethylene over gallium oxide and gallium nitride using density functional theory, Mol. Catal. 482 (2020) 110606. https://doi.org/10.1016/j.mcat.2019.110606.

[43] K. Dutta, M. Shahryari, J. Kopyscinski, Direct Nonoxidative Methane Coupling to Ethylene over Gallium Nitride: A Catalyst Regeneration Study, Ind. Eng. Chem. Res. 59 (2020) 4245–4256. https://doi.org/10.1021/acs.iecr.9b05548.

[44] J. Guo, Z. Hou, J. Gao, X. Zheng, DRIFTS Study on Adsorption and Activation of CH4 and CO2 over Ni/SiO2 Catalyst with Various Ni Particle Sizes, Chinese J. Catal. 28 (2007) 22–26. https://doi.org/10.1016/s1872-2067(07)60009-6.

[45] G. Socrates, Infrared and Raman Characteristic Group Frequencies: Tables and Charts, 3rd Edition, 3rd ed., John Wiley & Sons, Ltd, 2004.

[46] K. Dutta, L. Li, P. Gupta, D.P. Gutierrez, J. Kopyscinski, Direct non-oxidative methane aromatization over gallium nitride catalyst in a continuous flow reactor, Catal. Commun. 106 (2018) 16–19. https://doi.org/10.1016/j.catcom.2017.12.005.

[47] F. Cárdenas-Lizana, D. Lamey, L. Kiwi-Minsker, M.A. Keane, Molybdenum nitrides: a study of synthesis variables and catalytic performance in acetylene hydrogenation, J. Mater. Sci. 53 (2018) 6707–6718. https://doi.org/10.1007/s10853-018-2009-x.

[48] D. Zhao, Triblock Copolymer Syntheses of Mesoporous Silica with Periodic 50&nbsp;to 300&nbsp;Angstrom Pores, Science (80-.). 279 (1998) 548–552. https://doi.org/10.1126/science.279.5350.548.

[49] M. Vasilopoulou, I. Kostis, A.M. Douvas, D.G. Georgiadou, A. Soultati, G. Papadimitropoulos, N.A. Stathopoulos, S.S. Savaidis, P. Argitis, D. Davazoglou, Vapor-deposited hydrogenated and oxygen-deficient molybdenum oxide thin films for application in organic optoelectronics, Surf. Coatings Technol. 230 (2013) 202–207. https://doi.org/10.1016/j.surfcoat.2013.05.033.

[50] W. Gruenert, A.Y. Stakheev, R. Feldhaus, K. Anders, E.S. Shpiro, K.M. Minachev, Analysis of molybdenum(3d) XPS spectra of supported molybdenum catalysts: an alternative approach, J. Phys. Chem. 95 (2002) 1323–1328. https://doi.org/10.1021/J100156A054.

[51] A. Shchukarev, D. Korolkov, XPS Study of group IA carbonates, Open Chem. 2 (2004) 347–362. https://doi.org/10.2478/BF02475578.

[52] G.M. Rignanese, A. Pasquarello, J.C. Charlier, X. Gonze, R. Car, Nitrogen incorporation at Si(001)- SiO2interfaces: Relation between N 1s core-level shifts and microscopic structure, Phys. Rev. Lett. 79 (1997) 5174–5177. https://doi.org/10.1103/PhysRevLett.79.5174.

[53] D. Ma, Y. Lu, L. Su, Z. Xu, Z. Tian, Y. Xu, L. Lin, X. Bao, Remarkable improvement on the methane aromatization reaction: A highly selective and coking-resistant catalyst, J. Phys. Chem. B. 106 (2002) 8524–8530. https://doi.org/10.1021/jp020166h.

[54] D. Ma, Y. Shu, M. Cheng, Y. Xu, X. Bao, On the induction period of methane aromatization over Mo-based catalysts, J. Catal. 194 (2000) 105–114. https://doi.org/10.1006/jcat.2000.2908.

[55] X. Zhu, K. Yu, J. Li, Y.-P. Zhang, Q. Xia, C. Liu, Thermogravimetric analysis of coke formation on plasma treated Mo-Fe/HZSM-5 catalyst during non-oxidative aromatization of methane, React. Kinet. Catal. Lett. 87 (2005) 93–99. https://doi.org/10.1007/s11144-006-0013-7.

[56] C. Guizani, F.J. Escudero Sanz, S. Salvador, The nature of the deposited carbon at methane cracking over a nickel loaded wood-char, Comptes Rendus Chim. 19 (2016) 423–432. https://doi.org/10.1016/j.crci.2015.10.009.

Appendix

SEM images

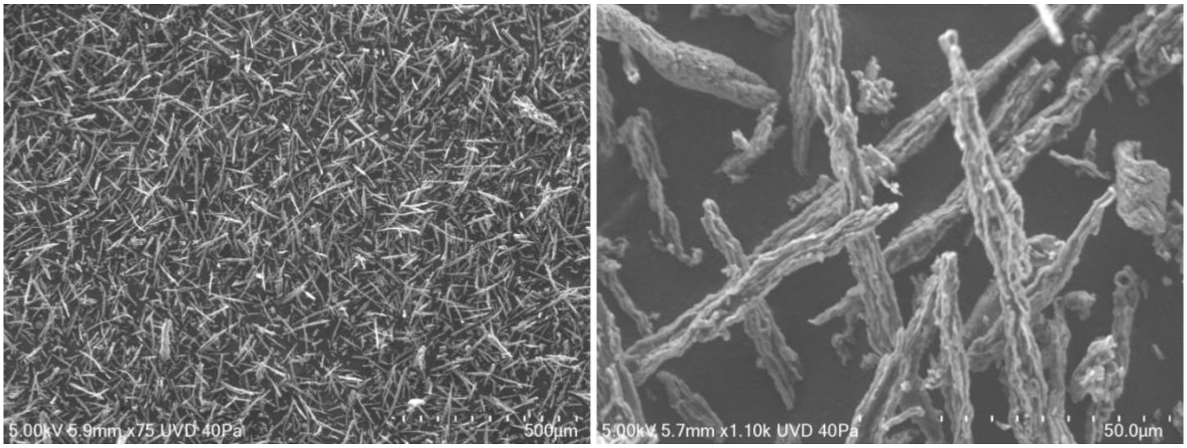

Fig. A-1: SEM of precious batch synthesized SBA-15.

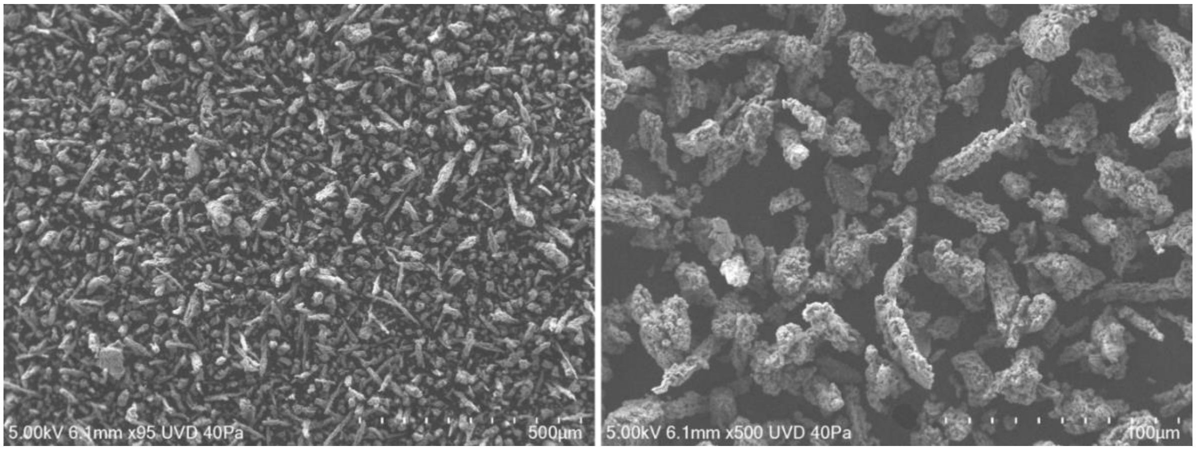

Fig. A-2: SEM of batch 1 synthesized SBA-15.

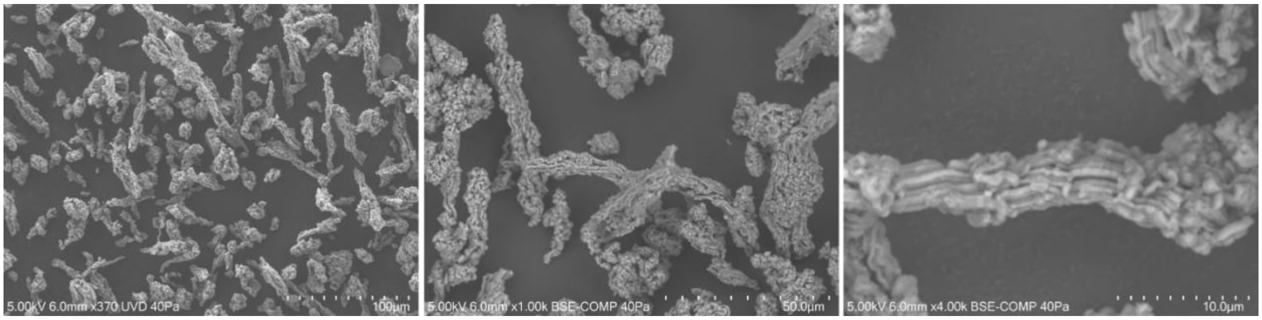

Fig. A-3: SEM of batch 2 synthesized SBA-15.

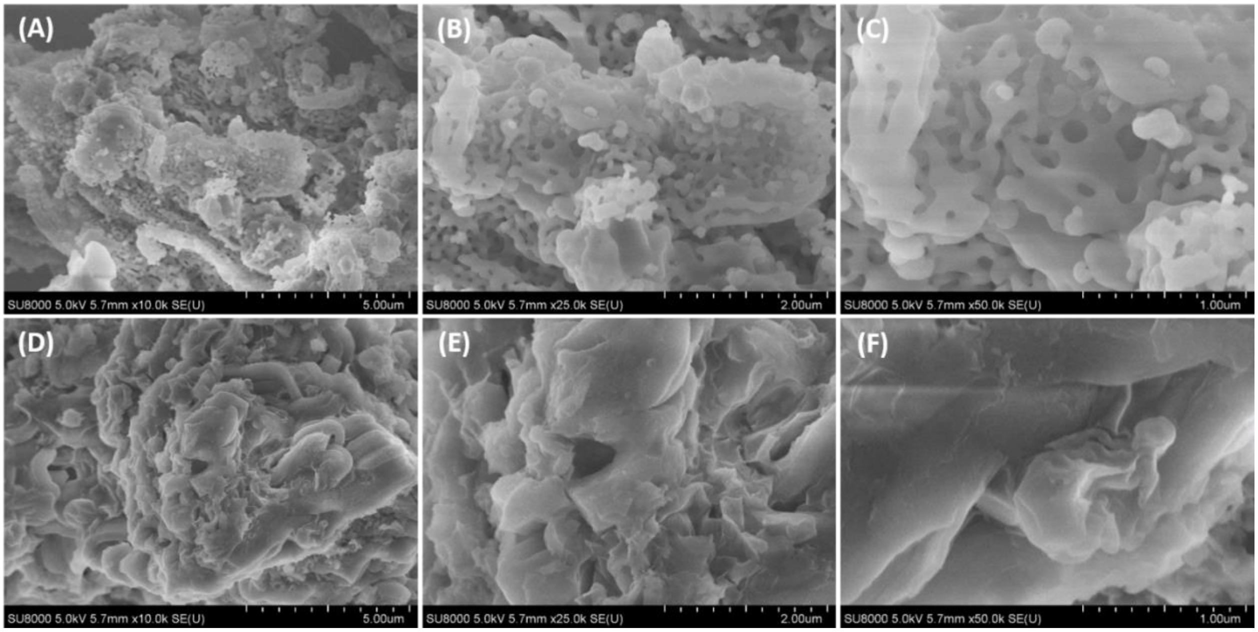

Fig. A-4: SEM images of spent (A–C) MoN and (D–F) WN catalysts.

XPS

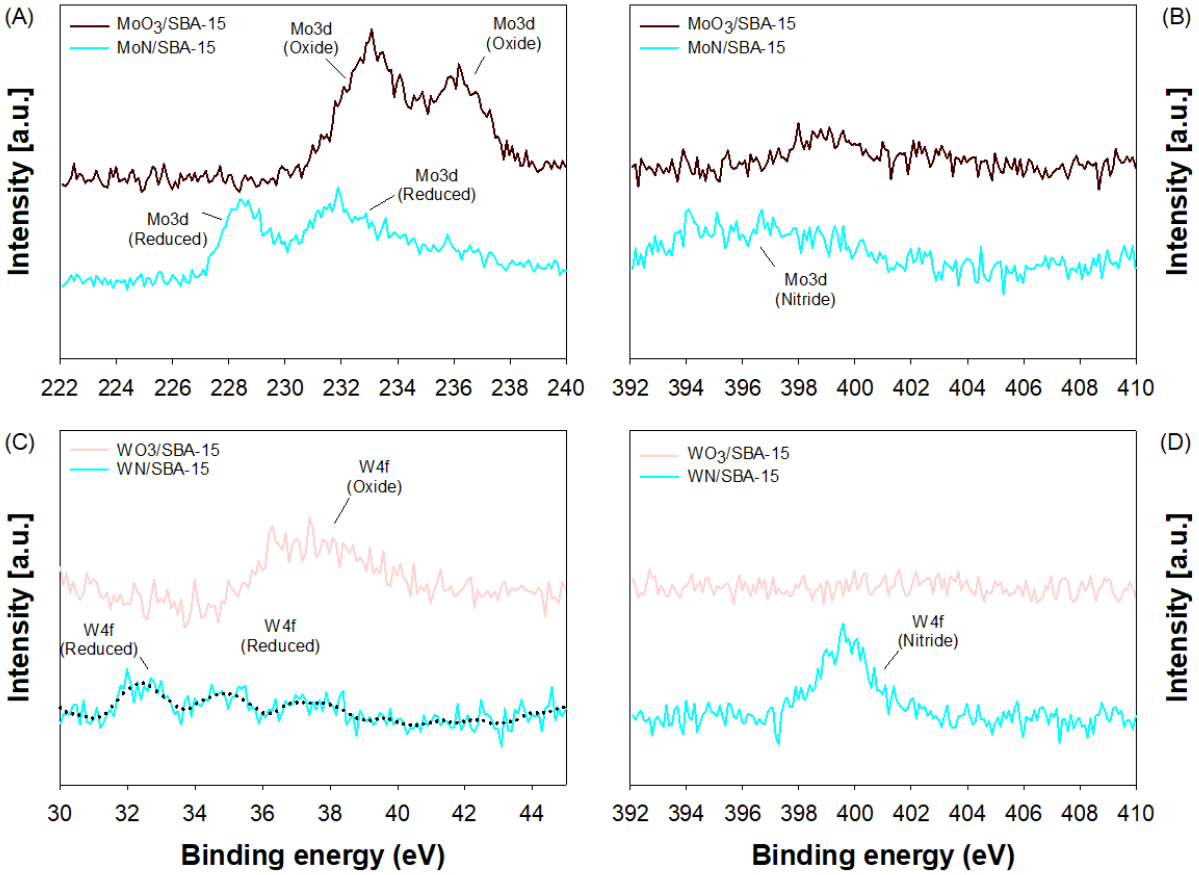

Fig. A-5: XPS plot of catalyst with 4 wt% loading for (A) molybdenum oxide and nitride catalysts showing Mo and (B) N spectra. Plots (C) shows tungsten oxide and nitride catalyst peaks corresponding to W and (D) N spectra. Dotted lines are for guidance only.

Activity

Conversion profile

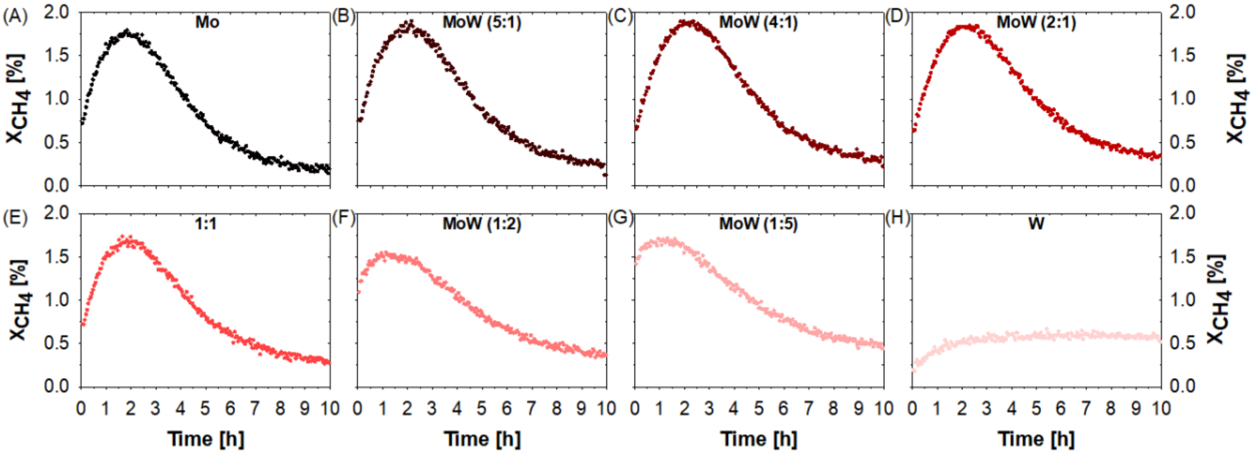

Fig. A-6: Conversion as a function of time on stream [h] for single and mixed-metal oxide catalysts activated with 50 vol% CH$_4$ (total = 8 ml min^{-1}) at 700 °C.

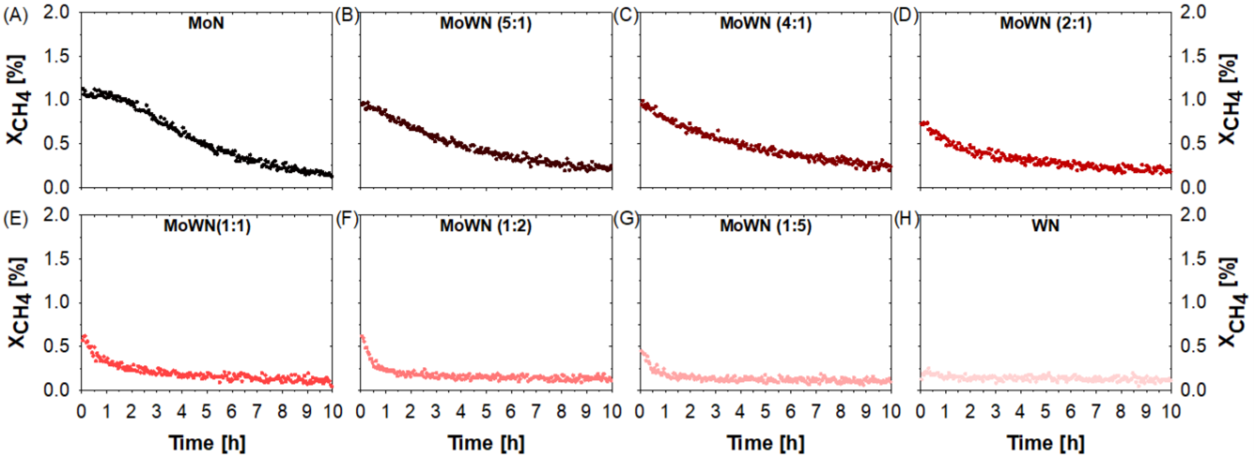

Fig. A-7: Conversion as a function of time on stream [h] for single and mixed-metal nitride catalysts activated with 50 vol% CH$_4$ (total = 8 ml min^{-1}) at 700 °C.

Selectivity profile

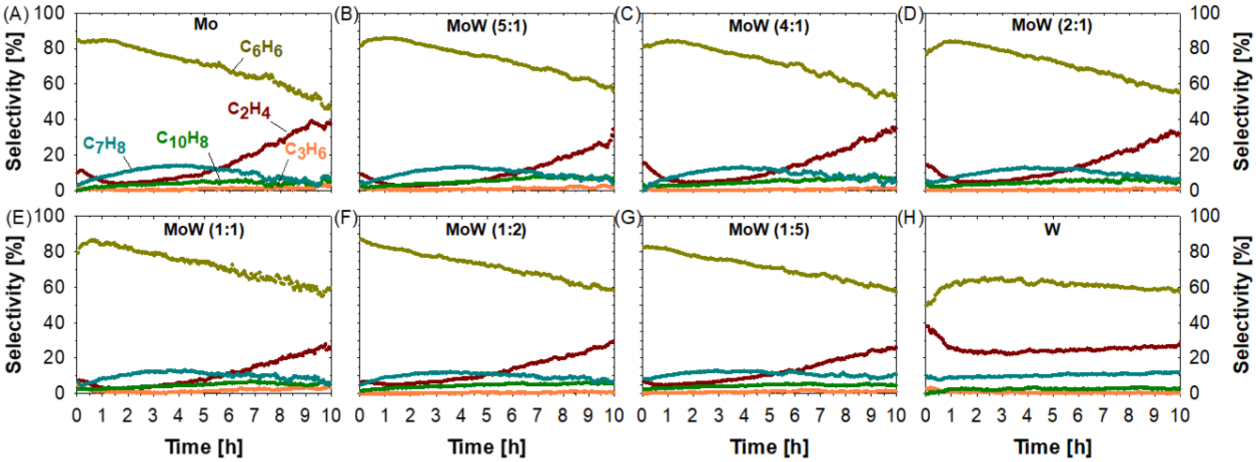

Fig. A-8: Selectivity as a function of time on stream [h] for metal and mixed-metal oxide catalysts activated with 50 vol% CH_4 (total = 8 ml min^{-1}) at 700 °C.

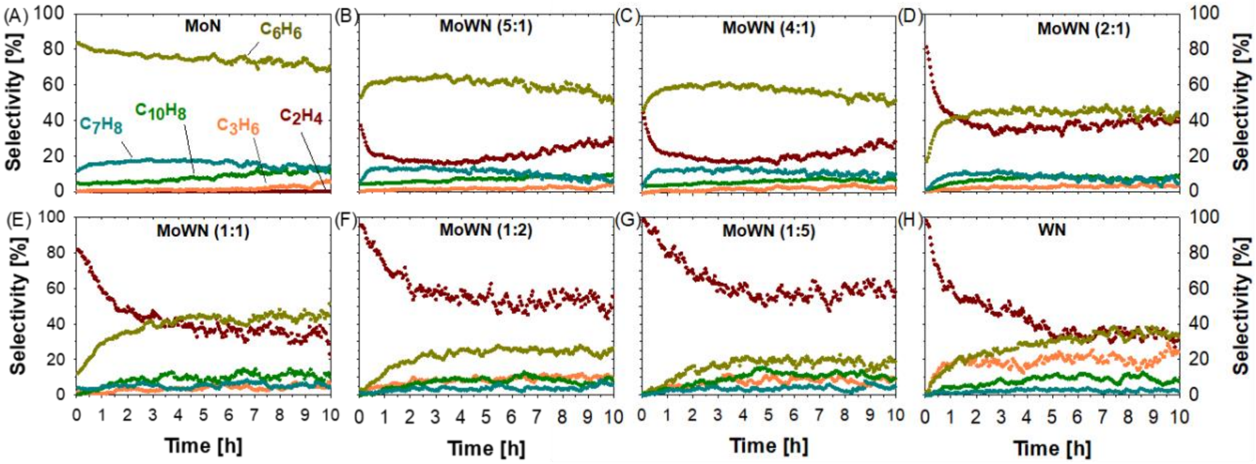

Fig. A-9: Selectivity as a function of time on stream [h] for metal and mixed-metal nitride catalysts activated with 50 vol% CH_4 (total = 8 ml min^{-1}) at 700 °C.

Nitridation

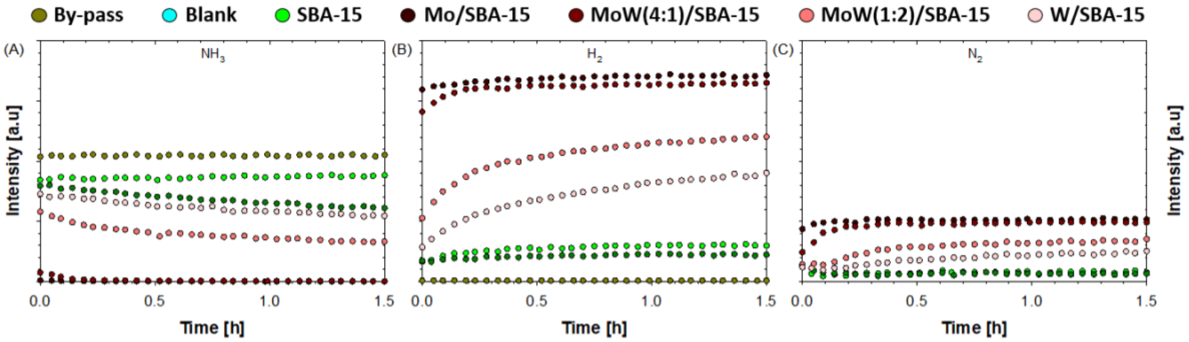

Fig. A-10: Effect of Mo loading on dehydrogenation of ammonia ($2NH_3 \rightarrow 3H_2 + N_2$). Signal intensity for (A) ammonia (B)hydrogen and (C) nitrogen during nitridation at 700 °C with 50 vol% NH_3 with balance Ar (total flow = 8 ml_N min^{-1}).